

# **ELECTROLESS Ni-B COATINGS: CONTROLLING FACTORS OF CARBON IN ITS COMPOSITIONS**

**M. Tech. Thesis**

By  
**MAHESH MALVIY**  
**(Roll No.: 2202103014)**



**DEPARTMENT OF MECHANICAL ENGINEERING  
INDIAN INSTITUTE OF TECHNOLOGY INDORE**

JUNE 2024

# **ELECTROLESS Ni-B COATINGS: CONTROLLING FACTORS OF CARBON IN ITS COMPOSITIONS**

**A THESIS**

*Submitted in partial fulfillment of the  
requirements for the award of the degree  
of*  
**Master of Technology**

*by*  
**MAHESH MALVIY**



**DEPARTMENT OF MECHANICAL ENGINEERING**  
**INDIAN INSTITUTE OF TECHNOLOGY INDORE**  
**JUNE 2024**

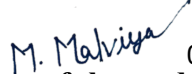


**INDIAN INSTITUTE OF TECHNOLOGY INDORE**

**CANDIDATE'S DECLARATION**

I hereby certify that the work which is being presented in the thesis entitled **ELECTROLESS Ni-B COATINGS: CONTROLLING FACTORS OF CARBON IN ITS COMPOSITIONS** in the partial fulfillment of the requirements for the award of the degree of **MASTER OF TECHNOLOGY** and submitted in the **DEPARTMENT OF MECHANICAL ENGINEERING, Indian Institute of Technology Indore**, is an authentic record of my own work carried out during the time period from July 2022 of joining the M.Tech. program to June 2024 of M. Tech. Thesis submission under the supervision of Dr. Satyajit Chatterjee, Professor Department of Mechanical Engineering and Dr. Suman Mukhopadhyay, Professor, Department of Chemistry.

The matter presented in this thesis has not been submitted by me for the award of any other degree of this or any other institute.

  
05-June-2024  
**Signature of the student with date**  
**(Mahesh Malviy)**

-----  
This is to certify that the above statement made by the candidate is correct to the best of my/our knowledge.

  
06.06.2024  
Signature of the Supervisor of  
M.Tech. thesis #1 (with date)  
**(Prof. Satyajit Chatterjee)**

  
06.06.24  
Signature of the Supervisor of  
M.Tech. thesis #2 (with date)  
**(Prof. Suman Mukhopadhyay)**

-----  
**Mahesh Malviy** has successfully given his M.Tech. Oral Examination held on **3<sup>rd</sup> June 2024**.

Signature(s) of Supervisor(s) of M.Tech. thesis  
Date:

  
Convener, DPGC  
Date: 06-06-2024

## ACKNOWLEDGEMENTS

First and foremost, I would like to express my heartfelt gratitude to my supervisor Dr. Satyajit Chatterjee, Professor, Department of Mechanical Engineering, Indian Institute of Technology, Indore, for his continuous support, valuable guidance, endless motivation, and encouragement throughout my M. Tech project. I was able to carry out my research work successfully because of his calm demeanor and excellent way to simplify things. I am indebted to him for sharing his valuable knowledge in the field of electroless coatings and tribology. His regular guidance and conversations assisted me in navigating through several challenging circumstances. I would also like to extend my sincere thanks to my co-supervisor, Dr. Suman Mukhopadhyay, Professor, Department of Chemistry, Indian Institute of Technology, Indore, for his continuous support in my project work.

I express my profound thankfulness to Arnott Inc. for sponsoring my M. Tech and providing me with all the necessary support during my research and academic work. The resources and opportunities offered by the company have significantly contributed to the success of my work. I am particularly grateful to Mr. M K Sathya, Mr. Dan Wallace, Mr. Brian Bitney, Ms. Meredith Kerr, and Mr. Kiran Kulkarni for their guidance and for facilitating a conducive environment for my studies. I would also like to thank Expert Global Solutions and all my colleagues who helped me directly and indirectly to complete my M. Tech.

I am also indebted to my family and my dearest friend Sourabh Shukla for their unwavering support and encouragement. Their faith in me has been a constant source of strength.

Finally, I would like to thank all my seniors, lab mates and colleagues, especially Dr. Vaibhav Nemane, Dr. Shahid Hussain, Mr. Setu Suman, and Mr. Dhruvil Thakkar for their camaraderie and for creating an inspiring and collaborative academic environment.

With Regards,

Mahesh Malviy

## DEDICATION

*Dedicated to*

*Mr. M K Sathya, a true mentor, and source of inspiration. With deepest gratitude for your unwavering belief in me, your support and encouragement have been invaluable in the completion of my M. Tech.*

## **Abstract**

The concept of electroless coating, a method of depositing a metal or alloy onto a substrate through a chemical reduction process without the use of an external power source. Electroless coating, a crucial technology in the field of surface engineering, offers uniform coating thickness, offers good corrosion resistance and excellent tribological properties. This M. Tech project research explores the study of electroless coatings fabricated on the low carbon steel substrates reduced by using sodium borohydride as reducing agent. Deposition process and the bath compositions conditions affect various factors influencing the composition of electroless coatings, aiming to optimize their properties for diverse industrial applications. The study systematically investigates the impact of key parameters, including temperature, pH, concentration of reactants, deposition time, and agitation, on the deposition rate and quality of the coatings. Through a combination of experimental methods and analytical techniques, this thesis identifies optimal conditions for achieving desired coating characteristics. The findings provide a comprehensive understanding of how these controlling factors interact, facilitating more precise control over the electroless coating process. This research not only contributes to the theoretical knowledge in the field but also offers practical guidelines for industrial applications, enhancing the performance and reliability of electroless coatings. The bath composition controlling the compositions of electroless Ni-B coatings has rarely been studied. In this project, attempts were made to study the composition of Ni-B coatings deposited in the electroless route and relate that to the composition of the bath solution in various stages. Before going to the mechanical and tribological tests, the electroless Ni-B coatings are thoroughly characterized using field emission scanning electron microscopy (FESEM), XRD analysis (X-ray Diffraction), Energy dispersive X-ray spectroscopy (EDS) and Inductive coupled plasma atomic emission spectroscopy (ICP-AES) by assessing the structural, compositional, and morphological features of the coatings. Furthermore, mechanical and tribological tests were done to understand the coatings behavior deposited with different factors.

# TABLE OF CONTENTS

CANDIDATE'S DECLARATION

ACKNOWLEDGMENTS

ABSTRACT

LIST OF FIGURES

LIST OF TABLES

NOMENCLATURE

## 1. Chapter 1: Introduction and Literature survey

### 1.1 Introduction

### 1.2 Classification of coating techniques

#### 1.2.1 Gaseous state coating type

1.2.1.1 Chemical vapor deposition (CVD)  
method

1.2.1.2 Physical vapor deposition (PVD) method

1.2.1.3 Ion Beam Assisted Deposition (IBAD)  
Coating Deposition method.

#### 1.2.2 Molten and semi-molten state techniques

#### 1.2.3 Solution state techniques

1.2.3.1 Electro-chemical deposition

1.2.3.2 Electroless or chemical solution  
deposition coating

### 1.3 Electroless coatings Overview and advantages

### 1.4 Engineering applications of coatings

### 1.5 Possible deposition by electroless coatings

#### 1.5.1 Chemistry and role of coating bath constituents

### 1.6 Reduction potential

### 1.7 Electroless Ni-B coatings bath chemistry

### 1.8 Tribological properties

### 1.9 Significance of Electroless Ni-B coatings reduced through borohydride.

### 1.10 Problem definition and objectives

### 1.11 Work plan.

## 2 Chapter 2: Experimental details

### 2.1 Introduction

### 2.2 Fabrication of electroless coatings

#### 2.2.1 Substrate preparation

- 2.2.2 Experimental setup details and electroless bath preparation
  - 2.2.2.1 Electroless coatings experiments with different conditions.
- 2.2.3 Bath replenishment
- 2.2.4 Coated samples sectioning
- 2.2.5 Mounting
- 2.2.6 Polishing
- 2.3 Characterization of prepared Ni-B coatings
  - 2.3.1 FESEM microscopic analysis
  - 2.3.2 ICP-AES test (Inductive coupled plasma atomic emission spectroscopy)
  - 2.3.3 XRD analysis (X-ray Diffraction)
  - 2.3.4 Raman Spectroscopic analysis
  - 2.3.5 XPS analysis (X-ray photoelectron spectroscopy)
- 2.4 Mechanical and tribological characterization
  - 2.4.1 Vickers Microhardness test
  - 2.4.2 Scratch tests.
  - 2.4.3 Sliding Wear tests
- 3 Chapter 3: Development of electroless Ni-B coatings with different conditions, Basic, Mechanical and tribological characterization
  - 3.1 Basic characterization Introduction
  - 3.2 Experimental details
  - 3.3 Results and discussions
    - 3.3.1 FESEM microscopic analysis
    - 3.3.2 Coating thickness analysis & pH monitoring of the bath solution
    - 3.3.3 ICP-AES analysis
    - 3.3.4 XRD analysis
    - 3.3.5 EDS analysis
    - 3.3.6 Raman Spectroscopy
    - 3.3.7 XPS analysis
  - 3.4 Mechanical and tribological characterization Introduction
    - 3.4.1 Result and discussion

3.4.1.1 Vickers Microhardness test

3.4.1.2 Scratch tests

3.4.1.3 Sliding wear tests

4 Chapter 4: Overall conclusions and future work scope

4.1 Introduction

4.2 Conclusions

4.3 Scope for future work

References:

## TABLE OF FIGURES

Figure 1 Classification of various surface modification techniques.....	1
Figure 2 Classifications of various surface coating methods.....	2
Figure 3 Historical development of electroless plating processes.....	7
Figure 4 Possible deposition by electroless method.....	9
Figure 5 Substrate Preparation for Electroless Coating.....	18
Figure 6 Electroless coating bath setup for electroless deposition process.....	19
Figure 7 Experiment A electroless deposition setup.....	20
Figure 8 Experiment B electroless deposition setup.....	21
Figure 9 Experiment C electroless deposition setup.....	22
Figure 10 coated sample.....	23
Figure 11 High-Speed Cutting Machine.....	23
Figure 12 Hot Mounting Machine.....	24
Figure 13 Polishing Machine.....	24
Figure 14 Polished samples.....	24
Figure 15 Samples were hot mounted for Cross-sectional analysis.....	26
Figure 16 FESEM Supra 55.....	26
Figure 17 Optical Microscope: Olympus U-MSSPG, Japan.....	26
Figure 18 Micro Hardness Tester Mitutoyo, (HM-210).....	31
Figure 19 Scratch Tester DUCOM (TR-101).....	32
Figure 20 Sliding Wear test machine.....	32
Figure 21 Top Surface morphology of the Ni-B coating- Experiment A & B.....	34
Figure 22 Top Surface morphology of the Ni-B coating- Experiment C.....	34
Figure 23 Representative FESEM cross-sectional image of Ni-B coatings from experiments. .....	35
Figure 24 Cross sectional images of Experiments A & B.....	36
Figure 25 Cross sectional image of Experiment C.....	36
Figure 26 Experiment-A Deposition rates of samples.....	37
Figure 27 Experiment-B Deposition rates of samples.....	38
Figure 28 Experiment-C Deposition rates of samples.....	38
Figure 29 pH monitoring of all three experiments.....	40
Figure 30 XRD Analysis for experiment A.....	43
Figure 31 XRD Analysis for experiment B.....	43
Figure 32 XRD Analysis for experiment C.....	44
Figure 33 Crystallite size by Williamson-Hall calculation for experiments A, B & C.....	46
Figure 34 Representative image of EDS analysis of the experiments.....	47
Figure 35 Carbon wt% of all three experiments from EDS analysis.....	48
Figure 36 Raman Spectra of Electroless Ni-B Coatings with Different Deposition.....	50
Figure 37 XPS Spectra of Electroless Ni-B Coatings with Different Deposition conditions...	54
Figure 38 Cross section micro hardness at Hv0.03 load.....	56
Figure 39 compound hardness of experiment A samples to compare hardness of A2 and A3 at 30, 50, and 100-gram load.....	57
Figure 40 Scratch test- COF for Experiment A samples.....	58

Figure 41 Scratch test- COF for Experiment B samples.....	59
Figure 42 Scratch test- COF for Experiment C samples.....	59
Figure 43 Scratch hardness for all eight samples.....	60
Figure 44 Wear test- AVG. COF for experiments A, B & C.....	61

## LIST OF TABLES

Table 1 Engineering applications of electroless coating deposition.....	8
Table 2 Bath composition and role of constituents of Ni-B coatings .....	19
Table 3 Bath Replenishment.....	22
Table 4 Chemical composition of Ni-B coatings by ICP-AES analysis.....	41
Table 5 Crystal size is calculated by Williamson Hall calculation and Scherrer .....	45
Table 6 Elemental Composition of Electroless Ni-B Coatings from Experiments A, B&C ...	48
Table 7 Carbon D & G band raman shift for each samples .....	51
Table 8 Key Binding Energies and Elemental Ratios for Electroless Ni-B Coatings .....	52
Table 9 Cross section micro hardness at Hv0.03 load (30gram load). .....	56
Table 10 Scratch test parameters at RT .....	58
Table 11 Sliding wear test parameters .....	61

# CHAPTER 1

## Introduction and Literature Survey

---

### 1.1 Introduction

Surface engineering is a multidisciplinary domain dedicated to enhancing the performance, durability, and aesthetics of materials by altering their surface properties. This field employs a wide range of processes and techniques to modify the surface layer of a material, often leaving its bulk properties unchanged. These modifications encompass mechanical, chemical, thermal, and electrochemical treatments designed to improve attributes like wear resistance, corrosion resistance, hardness, and visual appeal. Techniques for surface modification include coatings/plating, heat treatments, surface hardening, laser treatment, and anodizing, among others. Surface modification can be classified into three categories as shown in Figure 1 [1].

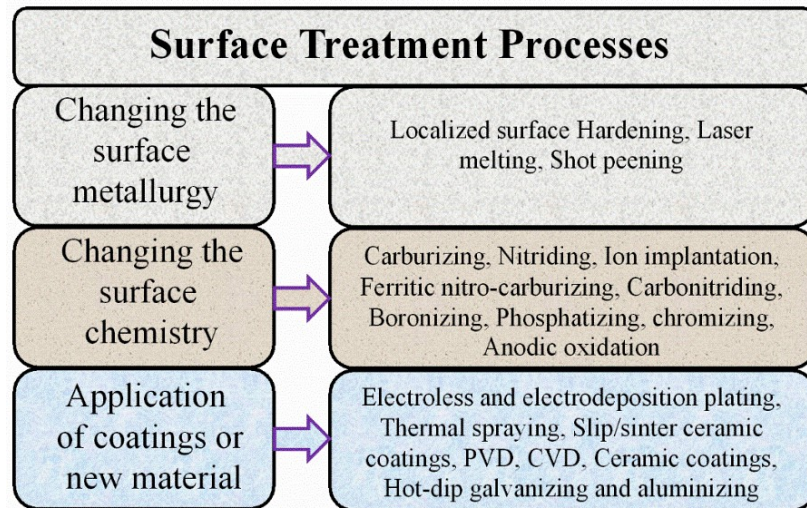


Figure 1 Classification of various surface modification techniques.

### 1.2 Classification of coating techniques

Coating techniques can be broadly classified based on the methods used to deposit the coating material onto the substrate. There are

various advanced techniques assisting in the components properties enhancements such as morphology, composition, structure, deposited thickness, and adhesion. According to the state and deposition mechanism. Figure 2 presents the general classification of various methods of surface coatings [2].

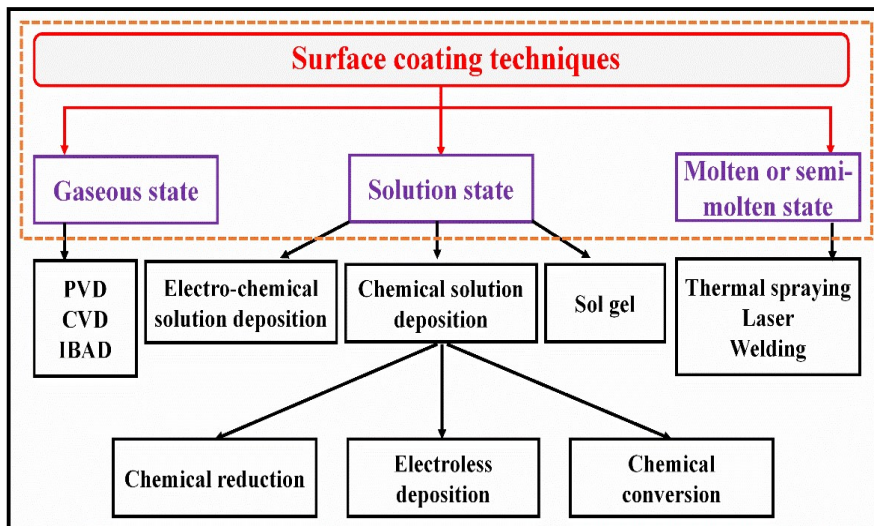


Figure 2 Classifications of various surface coating methods

## 1.2.1 Gaseous state coating type

Gaseous state coating refers to a class of coating techniques where the coating material is deposited from a gaseous phase onto a substrate. These methods are widely used in various industries due to their ability to produce high-quality, uniform, and adherent coatings. The two primary techniques in this category are Physical Vapor Deposition (PVD) and Chemical Vapor Deposition (CVD).

### 1.2.1.1 Chemical vapor deposition (CVD) method

CVD involves the chemical reactions of gaseous precursors that decompose or react on the substrate surface to form a solid film. The process can take place at various temperatures and often uses a heated substrate to drive the reactions [3]. There are few CVD techniques are available such as:

- a. Thermal CVD in which the substrate is heated to a high temperature, and gaseous precursors react to deposit the coating material.
- b. Plasma-Enhanced CVD (PECVD) in which plasma is used to enhance chemical reactions at lower temperatures compared to thermal CVD.

#### **1.2.1.2 Physical vapor deposition (PVD) method**

PVD encompasses several processes that involve the physical transfer of material from a condensed phase (solid or liquid) to a vapor phase and then to a thin film on a substrate [2]. The key PVD techniques are evaporation, sputtering and ion plating.

#### **1.2.1.3 Ion Beam Assisted Deposition (IBAD) Coating Deposition method.**

Ion Beam Assisted Deposition (IBAD) is a sophisticated coating technique that combines physical vapor deposition (PVD) with concurrent ion bombardment to enhance the properties of the deposited films. This method allows precise control over the film's microstructure, composition, and stress, making it highly suitable for advanced technological applications.

#### **1.2.2 Molten and semi-molten state techniques**

In this technique coatings can be fabricated in the molten or semi-molten state (or mixed state) of coating materials. Various anti-wear coatings can be prepared by these techniques, such as thermal spraying, laser assisted depositions, weld hard facing.

#### **1.2.3 Solution state techniques**

Solution state technique coatings involve the application of a coating material from a liquid solution onto a substrate. These methods are commonly used due to their simplicity, cost-effectiveness, and versatility. The coating material is typically

dissolved or suspended in a coating bath solution (aqueous) to deposit coating layer onto the substrate material with the reduction of metallic ions. Coatings can be fabricated on metallic or non-metallic specimens by using suitable methods. There are various categories available such as sol gel processing, dip coating, spin coating, and chemical deposition. The major advantages of the solution state processes is that the uniform and desired coating thickness can be achieved, unlike the gaseous state techniques, where the deposition rate and diffusion limited, deposition time is also higher, stresses and heat dissipation limits the desired coating thickness.

Majorly, electro plating and electroless plating techniques are widely used in manufacturing protective coatings on components [1, 2].

#### **1.2.3.1 Electro-chemical deposition**

Electrochemical deposition is a process in which metal ions are reduced to form a metal layer on the cathode (the substrate to be coated) by passing an electric current through an electrolyte solution containing those ions. The metal ions migrate towards the cathode and adhere to its surface. For successful deposition of a metallic or alloy coating, the substrate must be electrically conductive. This method relies on the principles of electrolysis and requires an external electric power source for deposition [1]. The electrodeposited layers are typically employed to enhance corrosion and wear resistance, for decorative purposes, and to increase heat tolerance. Chromium coating, often referred to as "Hard chrome," is one of the common electrodeposited coatings used in tribological applications due to its excellent friction and abrasion resistance properties. However, a significant limitation of electroplating is the difficulty in achieving uniform coatings on parts or components with complex geometrical shapes. [4].

### **1.2.3.2 Electroless or chemical solution deposition coating**

Electroless coatings, also known as autocatalytic coatings, represent a metal finishing method that deposits a metal layer on a substrate independently of an external electric power source. This process utilizes a chemical reduction reaction in an aqueous solution, allowing metal ions to be reduced and deposited on the substrate's surface. This technique, often termed chemical rather than electrochemical, underscores the lack of an electrical power source, though the deposition mechanism can still be analyzed through the lens of electrochemical redox potential [5].

The electroless or autocatalytic method offers significant flexibility in coating thickness and conformity, regardless of the substrate's shape. It is particularly effective for applying uniform, hard, and wear-resistant coatings on a variety of materials, including both metallic and non-metallic substrates. The influence of wear and corrosion on the performance of engineering materials is substantial. Through the electroless method, pure metals, binary, and ternary alloy metals can be deposited. Notably, electroless nickel, nickel-based alloy, and composite coatings hold substantial commercial importance. Electroless Ni-B coatings, in particular, are renowned for their exceptional tribological and wear resistance properties. These coatings typically display a mix of amorphous and crystalline structural characteristics, offering superior hardness and tribological performance compared to other commonly used compositions, which has led to their significant industry acceptance and popularity [6].

## **1.3 Electroless coatings Overview and advantages**

The process of electroless coating deposition was first discovered by Wurtz in 1844. Wurtz found that nickel could be deposited from a solution containing nickel salts reduced by hypophosphite, an occurrence initially seen as an anomaly due to its unexpected chemical nature: the nickel reduced to a powdery form that settled at the bottom of the container [5]. Despite this early discovery, the process did not

find any practical industrial applications at the time. It was not until World War II that the process gained industrial relevance when the American National Bureau of Standards (ANBS) began efforts to improve firearms. In a significant advancement in 1944, Brenner and Riddle, while at the ANBS, managed to produce a high-quality Ni-P alloy coating using a solution that exhibited remarkable stability [7,8]. Brinell is recognized as the “Father of electroless plating” within the surface finishing industries. The first electroless bath was prepared using a nickel salt solution with sodium hypophosphite as the reducing agent. Several years after the initial discovery, researchers explored the deposition of other alloys such as nickel-boron (Ni-B) and pure nickel using various reducing agents. In 1954, the creation of the first electroless bath using borohydride as a reducer marked a significant technological advancement, particularly during the years 1957 to 1958 [8]. Furthermore, in 1955, the first patent was issued for an electroless nickel-boron (Ni-B) plating process [9]. By 1967, electroless nickel plating was being produced with amine boron and sodium borohydride as reducing agents. While nickel-phosphorous (Ni-P) remains the most prevalent method for electroless plating, nickel-boron (Ni-B), which is the focus of this study, holds the second position and is highly preferred for its applications in numerous high-tech fields[10]. This study delves deeply into the nickel-boron alloy coating process, examining the factors that control its composition and the characteristics of the resulting coatings. Initially, it presents a theoretical overview of electroless deposition, followed by the experimental parameters and methods used for depositing nickel-boron. Detailed subsequent analyses will investigate the microstructural, mechanical, and tribological properties of these coatings. The historical evolution of electroless plating processes is depicted in Figure 3[5, 8].

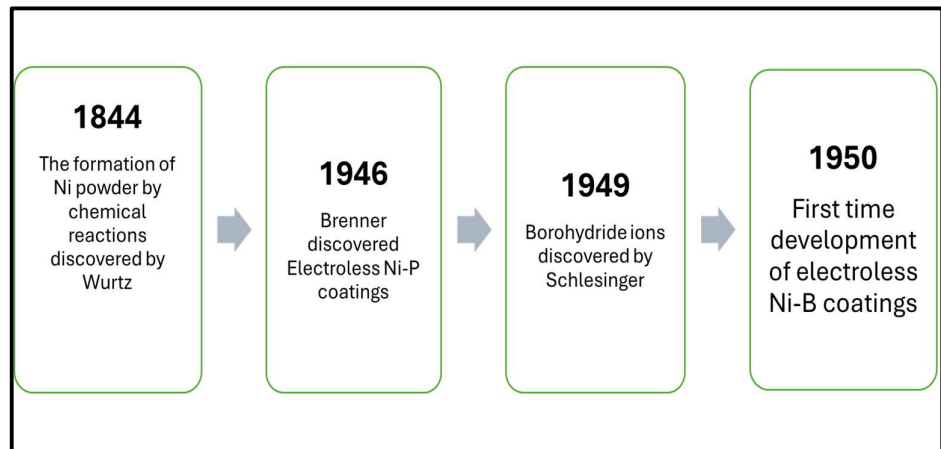


*Figure 3 Historical development of electroless plating processes*

There are various benefits of electroless plating/coatings over the traditional electro-deposition or electrolytic process and are presented as follows [5, 11]

**Uniform thickness:** It provides uniform coating thickness over the entire surface of the substrate including complex shape and geometry. It also provides lesser porosity which enhances the coating mechanical properties.

**No electric power, anode, batteries, or rectifiers needed for the electroless deposition.**

**Excellent adhesion:** The chemical reactions involved in the deposition process promote better molecular bonding which enhances the durability & longevity of coatings.

**This process is good for mass production because of its simple set-up as compared to electroplating.**

These coatings offer excellent tribological, mechanical, wear resistant, and corrosion resistant properties. Because of these qualities electroless coatings have a wider range of applications in almost all the industries.

Electroless deposition can be done on conductive and non-conductive substrate surfaces. The only requirement is that the substrate surface should be catalytically activated.

However, by varying the coating bath constituents, bath conditions and process parameters such as pH, temperature, deposition time desired coating characteristics can be achieved.

### 1.4 Engineering applications of coatings

Because of their excellent properties these coatings are used in most industries. There are some of the engineering applications shown in the table below [12]:

<b>Industries</b>	<b>Applications</b>	<b>Coating thickness</b>
Automotive Industries	Coatings for engine parts, fuel injectors, and other components requiring wear and corrosion resistance.	2–38 $\mu\text{m}$
Aerospace industries	Coatings for landing gear, turbine blades, and other critical components	10–50 $\mu\text{m}$
Electronics Industry	Coatings for PCBs, connectors, and other electronic components	12–25 $\mu\text{m}$
Oil and Gas Industry	Protective coatings for pipes, valves, and other equipment exposed to corrosive environments.	25–50 $\mu\text{m}$
Medical devices	Coatings for surgical instruments and implants that require biocompatibility and corrosion resistance	12–25 $\mu\text{m}$
Military	Fuse assemblies, tank tarred bearings, radar wave guides, mirrors, motors, detonators and firearms	8–75 $\mu\text{m}$
Mining	Hydraulic systems, jetting pump heads, mine engine components, piping connections, framing hardware	30–60 $\mu\text{m}$
Rail road	Tank cars, diesel engine shafts and car hardware	20–90 $\mu\text{m}$
Moulds & dies	Zinc dies, cast dies, glass moulds and plastic injection moulds of plastic extrusion dies	15–50 $\mu\text{m}$
Food Industries	Pneumatic canning machinery, baking pans, moulds, grills and freezers, mixing louts, bun warmers and feed screw and extruders	12–25 $\mu\text{m}$

*Table 1 Engineering applications of electroless coating deposition*

The versatility and performance benefits of electroless plating make it a valuable technique in a wide range of industries and applications.

### 1.5 Possible deposition by electroless coatings

Pure metals, binary metal alloys and multi alloy metals can be deposited through electroless route. The following figure 4 is showing the possible electroless deposition [5, 13].

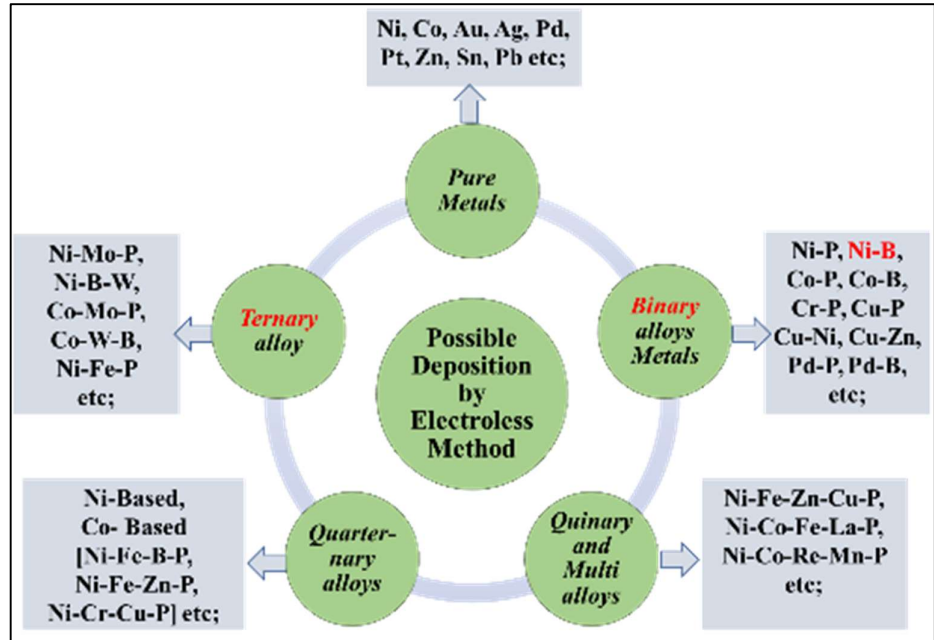


Figure 4 Possible deposition by electroless method

#### 1.5.1 Chemistry and role of coating bath constituents

Electroless bath solution contains various chemical constituents, and each one has an important role in the deposition process. This process relies on chemical reactions between the metal ions in the solution and a reducing agent. The chemistry and role of electroless coatings are multifaceted and offer numerous benefits across various industries. Electroless bath contains at least metal ion source, reducing agent, complexing agent, stabilizer and buffering agent or pH regulator. The function of each constituents explained here [5, 6, 10]

- A. **Metal Ion source:** Provides metal ions for coating. Commonly used metal salts include nickel chloride ( $\text{NiCl}_2$ ), nickel sulphate and sometimes nickel acetate for nickel plating but nickel acetate is very limited in use.
- B. **Reducing agent:** It gets oxidized in suitable conditions and provide electrons to reduce the metal ions in the form of nickel metal onto the substrate surface. There are various reducing agents available for pure nickel hydrazine is used, for Ni-P deposition sodium hypophosphite is used. DMEB (Die methyl boron), DEAB (Dimethyldiborane) and sodium borohydride ( $\text{NaBH}_4$ ) are used for Ni-B coatings. Among all these reducing agents, borohydride is the strongest reducing agent for Ni reduction (600gram is needed to reduce 1kg of nickel). Also, Borohydride reducing agent Ni provides as deposited higher hardness and excellent tribological properties [8, 11, 13].
- C. **Complexing agent:** Keeps the metal ions in solution by forming stable complexes, preventing their premature precipitation. Examples include ethylenediamine (EDA), citrates, and EDTA. The complexing agent binds with the metal ions to keep them in solution until they are reduced.
- $$\text{Ni}^{2+} + \text{EDA} \rightarrow \text{Ni}(\text{EDA})^{2+}$$
- Complexing agent also adds buffering effect in the plating bath which helps to avoid sudden drop of pH of bath solution. Complexing agents also take part in the deposition rate, quality of deposits and reaction mechanism. The amount of complexing agent also decides the content of phosphorus and boron in the coating. Most popularly EDA is used in borohydride bath to reduce Nickel coatings.
- D. **Stabilizer:** Prevent unwanted side reactions and control the plating rate. Stabilizers can include lead or thiourea compounds. Higher concentrations of stabilizer can increase porosity in the coatings, slow down the deposition rate and affect the brightness of the deposit. The stabilizer amount should be low to avoid such defects in the coatings.

Heavy salts such as thallium acetate or thallium nitrate are the most efficient stabilizer agents, but they are more toxic in nature [14, 15, 16]. So, the suitable alternatives are lead tungstate or lead nitrate as they are less toxic [17, 18].

- E. **Buffering agent:** It is also called a pH regulator. Maintain the pH of the solution within the optimal range for plating. Common buffers include ammonium hydroxide and sodium hydroxide. Replenishment of buffering agent can be done during the deposition process to maintain the desired pH value of the bath solution if the pH is decreased [19].

Apart from these electroless bath constituents some agents can be added such as accelerating agents which will increase the deposition process and brightening agents or shining agents which will provide smooth or shining surface.

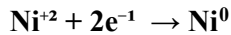
## 1.6 Reduction potential

It is also known as electrode potential or redox potential. It determines the feasibility and efficiency of the metal deposition reaction. This is the tendency of a chemical species to acquire electrons and be reduced. The reduction potential of the metal ions in the electroless solution determines how easily the metal can be deposited on a substrate.

The standard reduction potential of the metal ion needs to be more positive than the oxidation potential of the reducing agent for the reaction to proceed. It is denoted by  $E$  and measured in volts (V) and this reduction potential can be calculated with reference to (SHE) Standard hydrogen electrode. Under standard conditions the standard reduction potential is: 1 M concentration for each ion participating in the reaction, a pressure of 1 atm for any gases involved, and a temperature of 25°C (298 K).

## 1.7 Electroless Ni-B coatings bath chemistry

- a. **Metal Ions** from Metal Salt Nickel Chloride ( $\text{NiCl}_2 \cdot 6\text{H}_2\text{O}$ ) produce nickel ions which get reduced in form of coating at substrate surface.



- b. **Reducing Agent:** Oxidation of reducing agent and provide borohydride ions ( $\text{BH}_4^-$ )



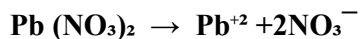
The Ni-B coating formation- overall equation:



- c. **Complexing agent as Ethylenediamine (EDA)** makes metal ion complex for controlled deposition:



- d. **Stabilizer (Lead Nitrite)  $\text{Pb}(\text{NO}_3)_2$**  : prevent the spontaneous decomposition of borohydride and control the deposition rate. It can also form a passivating layer on the nickel surface, preventing excessive hydrogen evolution which can cause pitting and poor quality of the coating.



These nitrite ions can help in redox reaction to reduce borohydride. [5]

## 1.8 Tribological properties

Tribology is the interdisciplinary study of the principles of friction, lubrication, and wear between interacting surfaces in relative motion. This field integrates aspects of mechanical engineering, materials science, physics, and chemistry to understand and improve the performance and longevity of mechanical systems. The word "Tribology" came from the Greek word "Tribos" that means rubbing or sliding.

Tribology plays a vital role in various fields, including mechanical design, biomedical fields, energy sector, manufacturing, and engineering materials science. Tribology helps to determine and enhance the components performance, efficiency, reliability, and life span of the components by analyzing tribological results. By understanding and controlling friction, lubrication, and wear, tribologists contribute to the development of more efficient, reliable, and longer-lasting machinery, thereby supporting advancements across various industries.

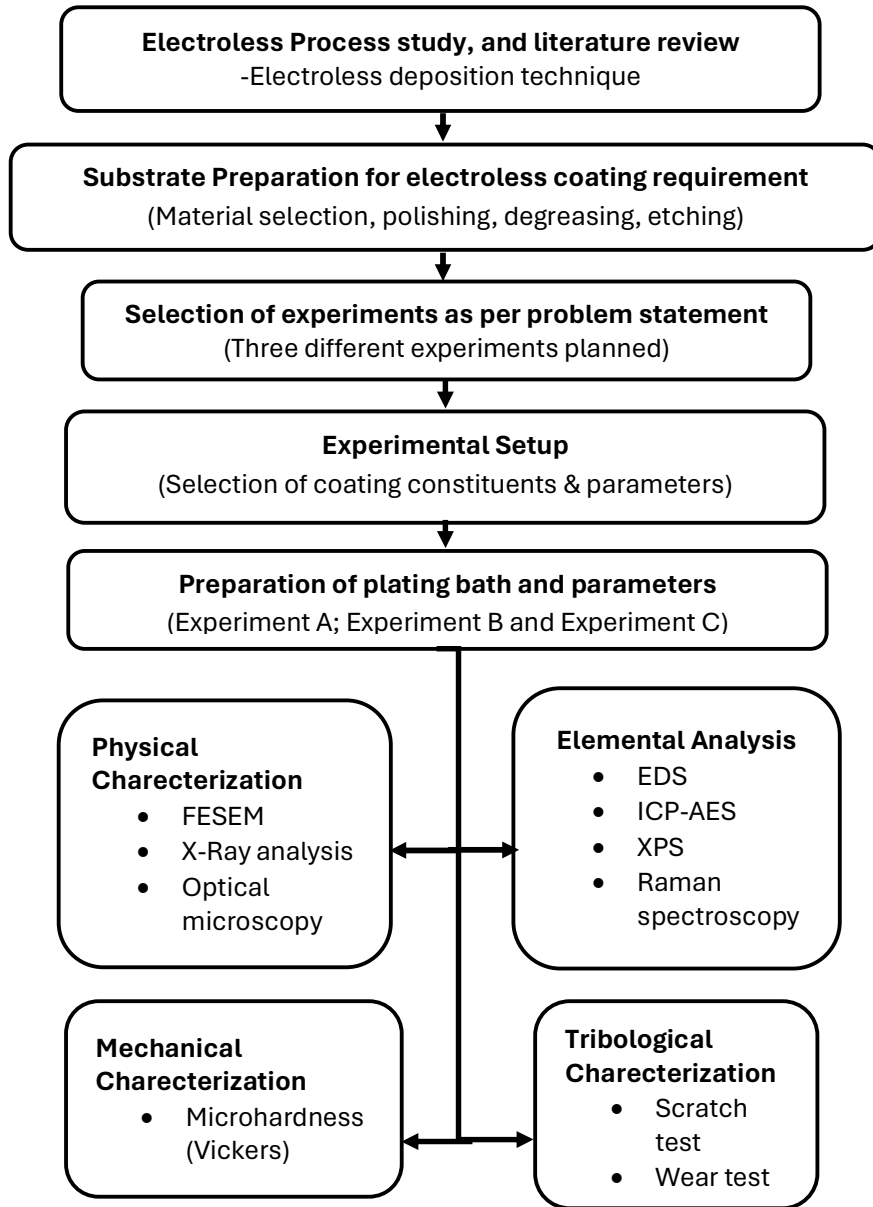
### **1.9 Significance of Electroless Ni-B coatings reduced through borohydride.**

Electroless Ni-B coatings reduced through borohydride hold significant importance in various industrial applications due to their unique properties and advantages over the other coatings. These coatings are known for their excellent tribological and mechanical properties, which make them ideal for use in almost all of the industries and critical mechanical components. The use of borohydride as a reducing agent in the electroless deposition process is particularly advantageous because it facilitates the formation of a uniform thickness, amorphous nickel-boron alloy coating without an external power source. This method also allows for the coating of complex shapes and provides a more consistent thickness compared to electroplating techniques. Research has shown that these coatings can significantly enhance the lifespan and performance of components in industries such as aerospace, automotive, and electronics [11, 29]. Additionally, the ability to control the boron content and deposition parameters enables the tailoring of coating properties to meet specific application requirements, further underscoring the versatility and significance of electroless Ni-B coatings reduced through borohydride.

## **1.10 Problem definition and objectives**

Many researchers have shown carbon content in the electroless Ni-B coating deposited using borohydride as a reducing agent, but there is very limited understanding of the source and the role of carbon present in this coating. The specific effects of carbon on the mechanical and tribological properties of electroless Ni-B coatings have not been thoroughly investigated yet. The objective of this project is to understand the origin and the role of carbon in influencing the physical characteristics and tribological performance of electroless Ni-B coatings. For this study, electroless Ni-B coatings are deposited using carefully chosen experimental parameters to closely observe the compositional variations in terms of mainly the carbon content. An effort to establish a relationship between this carbon content and coatings' mechanical and tribological properties is made. This study aims to provide insights about the electroless nickel based tribological coatings that could improve the scientific understanding about the coating and its application in various industrial sectors.

## 1.11 Work plan





## CHAPTER 2

### Experimental details

---

#### 2.1 Introduction

An overview of electroless Ni-B coatings has been covered in the previous chapter. Additionally, Chapter 1 includes a review of the literature, the project's novelty, its objectives, and the work plan. This chapter focuses on the experimental procedures followed and the material characterization techniques used for various analyses.

#### 2.2 Fabrication of electroless coatings

##### 2.2.1 Substrate preparation

Electroless Ni-B coating was applied to low carbon steel substrates (AISI 1025) of size 20 x 30 x 5 mm<sup>3</sup>. The samples were prepared using standard metallographic polishing with SiC abrasive papers ranging from 400 to 1200 grit to achieve a surface roughness of  $R_a \leq 0.5 \mu\text{m}$ . Notches were cut on one side of the samples to tie them during immersion in the coating bath with the help of thin wires. These polished samples underwent ultrasonic cleaning for 15 minutes, followed by a 10-minute dip in 10% NaOH solution at 50-60 °C for alkaline cleaning. The surfaces were then rinsed in 37% HCl for 15-20 seconds to remove oxides and activate the substrate surface before immersion in the electroless coating bath. This pretreatment process is essential for effective coating deposition, making the substrates ready for the coating process. Refer figure 5 for substrate preparation [24].

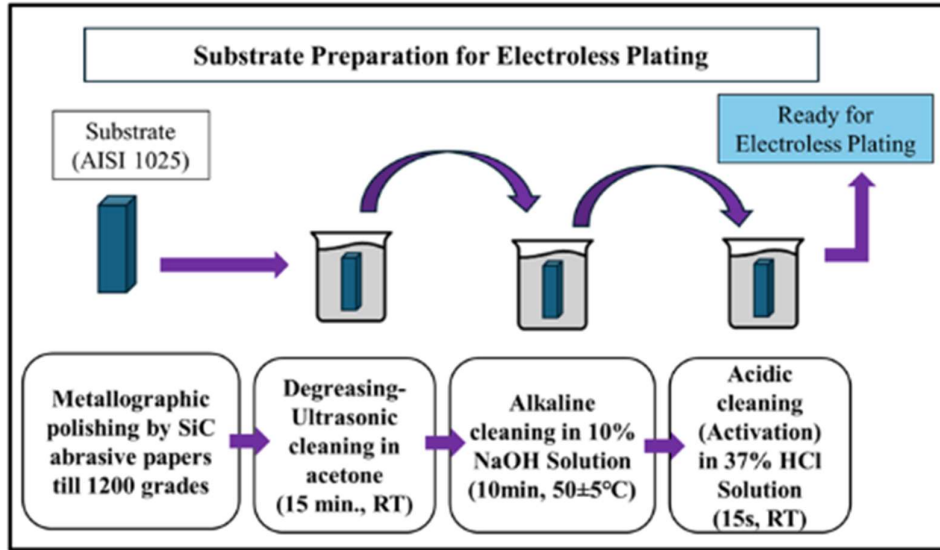


Figure 5 Substrate Preparation for Electroless Coating

## 2.2.2 Experimental setup details and electroless bath preparation

The electroless bath consists of Nickel chloride ( $\text{NiCl}_2 \cdot 6\text{H}_2\text{O}$ ) as the source of  $\text{Ni}^{2+}$  ions, Sodium borohydride ( $\text{NaBH}_4$ ) as the reducing agent, Ethylenediamine ( $\text{C}_2\text{H}_8\text{N}_2$ ) as the complexing agent, Sodium hydroxide ( $\text{NaOH}$ ) for buffering or pH regulation, and Lead nitrite ( $\text{Pb}(\text{NO}_3)_2$ ) as the stabilizer. Dissolve all the bath constituents in distilled water to prepare the electroless bath as per the process. Add sodium borohydride (the reducing agent) to the bath just before immersing the substrate in the coating solution. It is crucial to closely monitor process parameters, including pH and temperature. The pH is measured using a pH meter from EUTECH Instruments, made in Singapore, while the temperature of the solution is maintained at  $90 \pm 2$  °C and monitored with a thermometer from G H ZEAL LTD, London, England (76mm immersion,  $\text{N}_2$  filled). Temperature control is achieved using a magnetic stirrer with a hot ceramic plate (Cole Parmer, Model 15956-31). To ensure uniform distribution of the bath constituents, proper stirring is facilitated by the magnetic stirrer. Figure 6 illustrates the electroless coating bath setup for the deposition process. After the coating deposition is completed according to the

specified time, the specimen is removed from the bath solution, rinsed with deionized water, and dried.

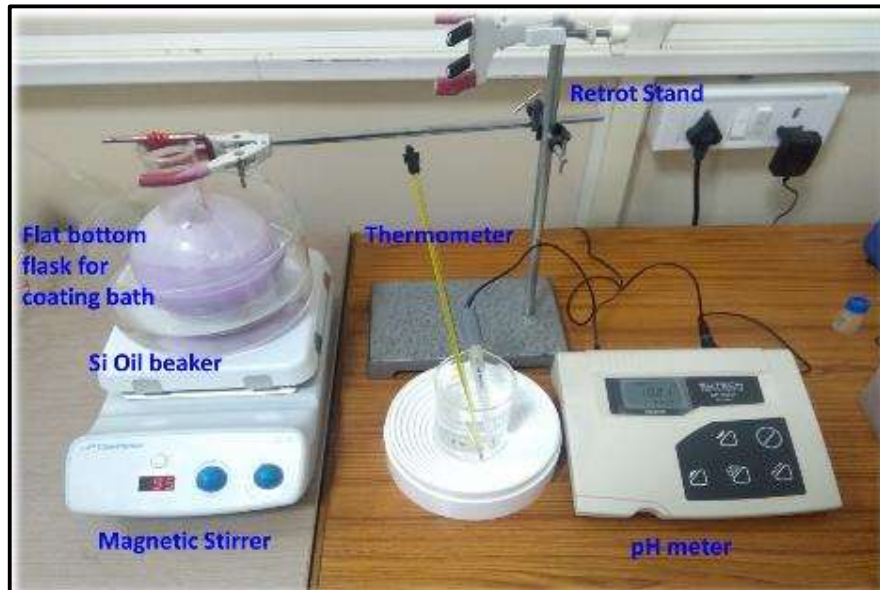


Figure 6 Electroless coating bath setup for electroless deposition process

### 2.2.2.1 Electroless coatings experiments with different conditions

The sequence of components for the electroless Ni-B bath composition used to deposit electroless Ni-B coatings is detailed in Table 2 below [24, 25].

Composition of bath solution	Role of the constituents	Qty
Nickel Chloride (NiCl <sub>2</sub> , 6H <sub>2</sub> O)	Metal ion source— Provides M <sup>+</sup> ions in coating bath	20 g/l
C <sub>2</sub> H <sub>8</sub> N <sub>2</sub> (Ethylenediamine)	Complexing agent — Prevent excess of free metal ions concentration by forming metal complex with metal ions	59 g/l
NaOH (Sodium hydroxide)	Buffer & pH regulator — Sustain the pH for long time & maintain pH(13±1)	20 g/l
Pb (NO <sub>3</sub> ) <sub>2</sub> (Lead Nitride)	Stabilizer — Stabilize the bath from spontaneous decomposition and controlling the deposition rate	0.0175 g/l
NaBH <sub>4</sub> (Sodium Borohydride)	Reducing agent —It gets oxidized and generate electrons to reduce the metal ions	0.8 g/l

Table 2 Bath composition and role of constituents of Ni-B coatings

Three distinct experimental conditions were selected for this project after thorough brainstorming. These conditions vary in deposition time, bath conditions over time, and the different immersion durations of the substrates.

- a. **Experiment A:** For this experiment, three substrates were utilized, each submerged in the bath solution for one hour to facilitate coating deposition. The total duration of coating deposition amounted to 180 minutes. Sample A1 was immersed in the bath solution at the onset of the deposition process, removed after 60 minutes, while Sample A2 was immersed during the second hour (immediately following the removal of A1) and kept for 60 minutes before being lifted out. Sample A3 was immersed into the coating bath after two hours of starting the deposition process, i.e. immediately after A2 was removed from the bath solution. Figure 7 below provides a comprehensive overview of the coating deposition process for samples A1, A2, and A3.

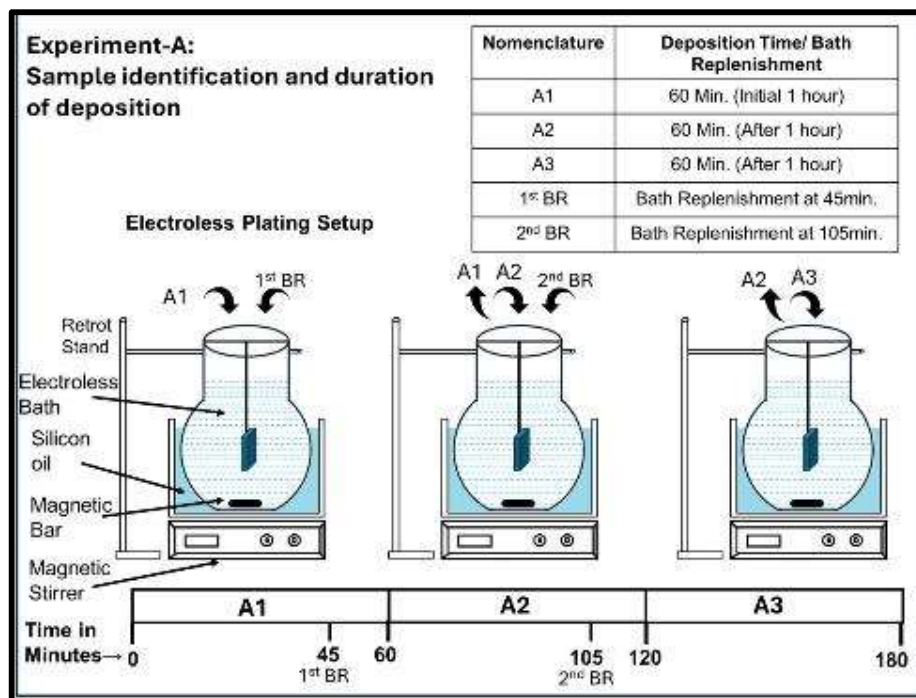


Figure 7 Experiment A electroless deposition setup

- b. **Experiment B:** Each of the three substrates was immersed in the coating bath at the start of the process. Sample B1 was removed after 60 minutes, B2 after 120 minutes, and B3 after 180 minutes. Figure 8 below provides a detailed overview of the coating deposition process for samples B1, B2, and B3.

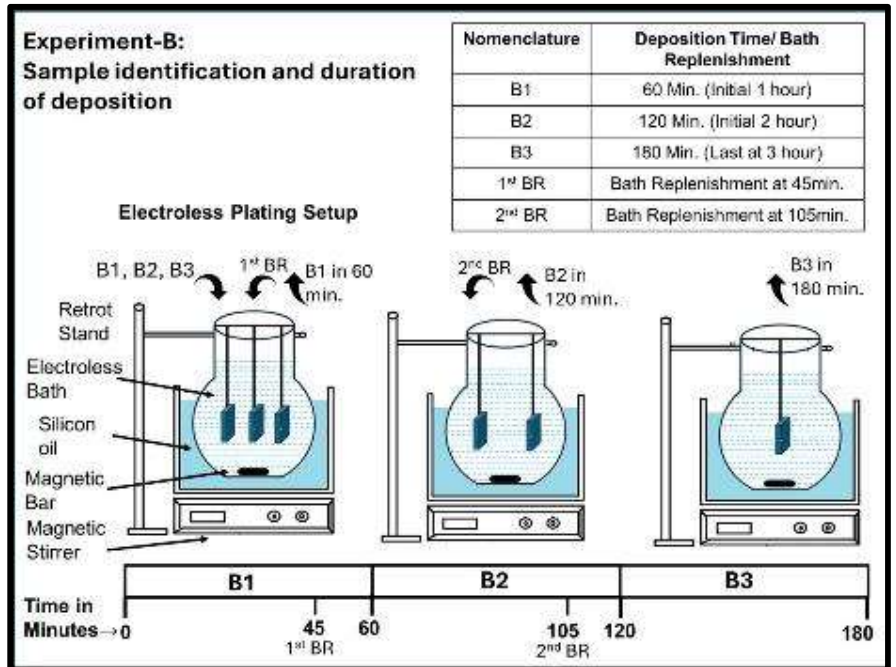


Figure 8 Experiment B electroless deposition setup

- c. **Experiment C:** Two substrates were selected for the coating deposition. Both C1 and C2 were immersed in the bath solution at the onset of the deposition process. C1 was removed after 60 minutes, while C2 was lifted off after 180 minutes (without bath replenishment).

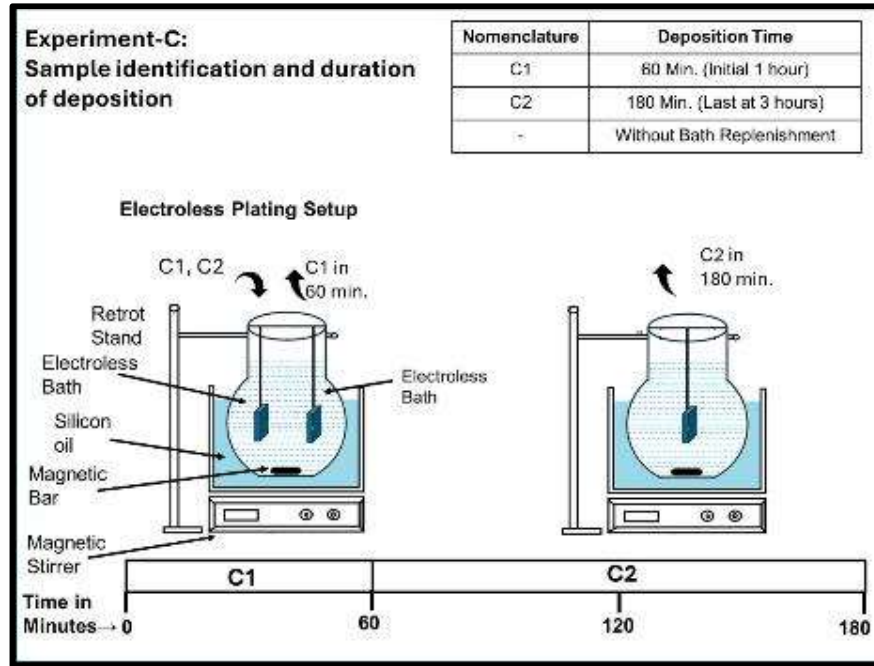


Figure 9 Experiment C electroless deposition setup

### 2.2.3 Bath Replenishment

To ensure the successful deposition of Ni-B coatings under three different coating bath conditions with varying deposition times, bath replenishment was performed. Half the quantity of the reducing agent (sodium borohydride) and stabilizer (Lead nitrite) were added at 45 minutes and 105 minutes to facilitate efficient coating deposition [24, 25].

Constituents	Concentration
Lead nitrate	0.00725g in 500ml bath
Sodium borohydride	0.2g in 500ml bath
Interval of replenishment (Time)	45, and 105 minutes

Table 3 Bath Replenishment

## 2.2.4 Coated samples sectioning

Following the coating deposition, the samples underwent ultrasonic cleaning in acetone for 5 minutes at room temperature. Please refer to figure 10 below for an image of the coated sample. Subsequently, the samples were sectioned into smaller pieces for characterization purposes using a High-Speed Cutting Machine (Struers Secotom-15) and wire-EDM (Electronica-ECOCUT).



*Figure 10 coated sample*



*Figure 11 High-Speed Cutting Machine*

## 2.2.5 Mounting

A small portion of samples from all substrates (A1, A2, A3, B1, B2, B3, & C1, C2) was mounted using a hot mounting machine (BUEHLER Simplimet 3000, Automatic mounting press). Hot

mounting is done to facilitate polishing and measure the coating thickness of all samples.



*Figure 12 Hot Mounting Machine*

## 2.2.6 Polishing

After mounting all the samples, standard metallographic methods were employed to polish them until achieving diamond polishing. This process allows for the examination of coating thickness and ensures that the polished surfaces are devoid of scratches or any defects, possessing a mirror-like finish. Polishing was carried out until diamond polishing using selvyt cloth and diamond paste with aerosol spray for lubrication.



*Figure 13 Polishing Machine*



*Figure 14 Polished samples*

## **2.3 Characterization of prepared Ni-B coatings**

### **2.3.1 FESEM microscopic analysis & EDS analysis**

Field Emission Scanning Electron Microscopy (FESEM) is an advanced imaging technique used to examine the surface morphology and microstructural details of materials with high resolution and magnification. This method is especially useful in materials science and engineering for analyzing coatings, thin films, and nanostructures. FESEM works by directing a focused beam of electrons from a field emission gun (FEG) onto the specimen's surface. The interaction between the electrons and the sample generates various signals, mainly secondary electrons, which are collected to produce high-resolution images. To understand the surface properties and microstructure of the as-deposited electroless Ni-B coatings, FESEM study is required.

FESEM analysis enables the observation of fine details and nanostructures within the coating, offering in-depth insights into both the surface topography and subsurface characteristics of the coatings.

Minimal sample preparation and the non-destructive nature of FESEM preserve the integrity of the samples. The Scanning Electron Microscope used (FESEM, Zeiss Supra-55) is equipped with an Energy Dispersive Spectroscopy (EDS) analyzer for microstructural analysis of the samples. The EDS detector, featuring an ultrathin window, can reliably detect elements heavier than beryllium. The acceleration voltage for the EDS analyzer is set at 20kV.



*Figure 15 Samples were hot mounted for Cross-sectional analysis*

All eight samples were cut and metallographically polished by hot mounting to check the cross-sectional thickness and for the microhardness. We have also measured the coating thickness by optical microscope (Olympus U-MSSPG, Japan)



*Figure 16 FESEM Supra 55*



*Figure 17 Optical Microscope: Olympus U-MSSPG, Japan*

### **2.3.2 ICP-AES test (Inductive coupled plasma atomic emission spectroscopy)**

A popular analytical method to detect elements and figuring out elemental concentrations in a variety of materials is Inductively Coupled Plasma-Atomic Emission Spectroscopy (ICP-AES), also known as Inductively Coupled Plasma-Optical Emission Spectroscopy (ICP-OES). This method is particularly useful for monitoring the deposition process and confirming the intended chemical composition of electroless Ni-B coatings by evaluating their composition. The atomic emission spectroscopy principle, which involves atomizing and ionizing the sample in a high-temperature plasma source, provides the foundation for how ICP-AES operates. The elemental composition of the sample is then ascertained by analyzing the light released by the excited atoms and ions.

ICP-AES is used to evaluate the concentrations of nickel (Ni), boron (B), and other elements in the coating material [25].

### **2.3.3 XRD analysis (X-ray Diffraction)**

XRD (X-ray Diffraction) is one of the powerful analytical techniques used to determine the phase composition, crystalline structure, and other structural characteristics. It is widely used for the investigation of metals, ceramics, polymers, and thin films, including electroless Ni-B coatings, in the domains of materials science, chemistry, and physics. The basis for X-ray scattering diagrams (XRD) is the constructive interference of monochromatic X-rays that are scattered by periodic atomic planes in crystalline materials. Three main parts comprise an XRD system: a sample holding, a detector, and an X-ray source.

A method for analyzing the phases and structural characteristics of crystalline materials in coatings is called X-ray diffraction, or XRD. The atomic arrangements can also be determined in amorphous materials. For this investigation, an Empyrean X-ray

diffractometer (Malvern Panalytical) equipped with Cu-K $\alpha$  radiation was used to conduct XRD analysis. For the Ni-B coating samples, the 2 $\theta$  scan range was set at a step size of 0.05, ranging from 20° to 80°.

In X-ray diffraction (XRD), Bragg's Law is utilized to establish a relationship between the X-ray wavelength ( $\lambda$ ), the crystal's interplanar spacing ( $d$ ), and the angle of incidence ( $\theta$ ).

$$n\lambda = 2d \sin\theta$$

where  $n$  is an integer representing the order of the reflected wave.

The XRD data was further analyzed with the help of X'Pert High score software (Philips Analytical B.V., Netherlands) and peaks are identified. Samples are cleaned by ultrasonic cleaning in the acetone before the test.

#### 2.3.4 Raman Spectroscopic analysis

Vibrational, rotational, and other low-frequency modes in a system can be studied analytically using Raman spectroscopy. It is frequently used to offer comprehensive details regarding the makeup, structure, and interactions of molecules in the fields of biology, chemistry, and materials science. Raman spectroscopy is remarkably useful for characterizing the chemical and structural properties of materials, including thin films, nanomaterials, and coatings like electroless Ni-B coatings.

The basis of Raman spectroscopy is the inelastic scattering of monochromatic light, typically emitted by a laser. Most photons are elastically scattered when light interacts with phonons or molecular vibrations in a material (Rayleigh scattering). However, due to the Raman effect, a tiny percentage of the light is inelastically scattered at energies that are either greater or lower than the incident light.

It includes:

- a. **Raman Shift:** The Raman shift is the energy difference between the incident photons and the dispersed photons. The

vibrational modes of the molecules in the sample are revealed by this shift.

**b. Raman Spectrum:** The Raman spectrum is a plot of intensity versus Raman shift (usually in wavenumbers,  $\text{cm}^{-1}$ ). Every peak in the spectrum represents a particular molecular vibrational mode. A non-destructive method for study of the availability of different phases in samples is Raman spectroscopy. Using a RAMAN Spectrometer, the Ni-B surfaces are analyzed using Raman spectroscopy in this study. (Horiba Scientific Mode: LabRAM HR Evolution Labram HR UV -VIS- NIR (220nm- 2200nm)).

### 2.3.5 XPS analysis (X-ray photoelectron spectroscopy)

X-ray Photoelectron Spectroscopy (XPS) is a surface-sensitive technique used to analyze the elemental composition, chemical state, and electronic state of materials. XPS is especially useful for characterizing thin films, coatings, and surface treatments, including electroless Ni-B coatings.

XPS works on the principle of the photoelectric effect, where X-rays irradiate a material, causing the emission of core electrons from surface atoms. The kinetic energy of these emitted electrons is measured, allowing for the determination of their binding energy.

The XPS principle includes:

- a. **Photoelectric Effect:** When X-rays hit a material, they can remove core-level electrons from the atoms.
- b. **Binding Energy:** It is possible to identify and measure the elements on the material's surface due to the binding energy, which is particular to certain elements and their chemical states.
- c. **Surface Sensitivity:** XPS is suitable for surface and thin film study because of its high surface sensitivity and ability to probe depths of 1 to 10 nanometers.

In the present study, XPS spectra of all N-B-coated samples are recorded (machine make- Kratos Analytical, UK SHIMADZU group: AXIS Supra) with a monochromatic radiation source of Al-K $\alpha$  (1486.6 eV). A specimen of size 2x2x2 mm<sup>3</sup> is prepared by sectioning and the flat bottom by polishing. The XPS chamber is under ultra-high vacuum conditions, and the pressure inside the sample loading chamber and the analyzer chamber was recorded as 1.2 x 10<sup>-8</sup> mbar, and 2 x 10<sup>-9</sup> mbar, respectively. The full-length scan was taken from 0 to 1200 eV binding energy.

## 2.4 Mechanical and tribological characterization

### 2.4.1 Vickers Microhardness test

The microhardness of the coating samples from the cross sections was taken from the Vickers microhardness test. The Vickers indenter is a pyramidal diamond in shape with a face angle of 136° and makes a square-shaped indent onto the surface. The hardness measurement was taken by Mitutoyo's (HM-210) hardness tester with loads of 30, 50, and 100 gf and a dwell time of 15 seconds. The Vickers hardness number is denoted by  $Hv$ , it is the ratio of applied load by the indentation to the surface area of the indentation mark. It is calculated by following formula:

$$Hv = \frac{2P \sin\left(\frac{\alpha}{2}\right)}{D^2}$$

Here,

D → Mean diagonal length of indentation mark (mm)

P → Applied Load (in kgf)

$Hv$  → Vickers hardness (kgf/mm<sup>2</sup> or GPa)

The mounted samples are metallographically polished, and an average of 10 readings are taken on the cross section of the coatings instead of the top surface to avoid compound hardness [24].



*Figure 18 Micro Hardness Tester Mitutoyo, (HM-210)*

#### **2.4.2 Scratch tests**

A scratch test is performed to see the coating's response to the scratching. Scratch hardness and fracture toughness properties are evaluated. A DUCOM (TR-101) scratch tester with a Rockwell C diamond indenter (Blue Star, apex angle:  $120^\circ$ , tip radius:  $200\mu\text{m}$ ) is used at room temperature.

Both constant and progressive scratch tests were performed with different loading conditions to check the adhesion of the coating to the substrate, and the coating was found to be well adherent. So, in this present study, unidirectional constant scratch tests were done multiple times at constant load and the coating behavior was analyzed under repetitive scratch testing [24, 25].



*Figure 19 Scratch Tester DUCOM (TR-101).*

### **2.4.3 Sliding Wear tests**



*Figure 20 Sliding Wear test machine*

## CHAPTER 3

### **Development of electroless Ni-B coatings with different conditions, Basic, Mechanical and tribological characterization**

---

#### **3.1 Basic characterization Introduction**

The previous chapter discussed the experimental aspects, including the development of the coating and a summary of the characterizations. All of the coating characterizations, including morphology, coating thickness, elemental analysis, and XRD, have been completed in this chapter.

#### **3.2 Experimental details**

The coatings are fabricated as explained in Chapter 2 and Section 2.2. Along with experimental details of physical characterizations, mechanical characterization, elemental analysis, experimental details, and tribological characterization have already been discussed.

#### **3.3 Results and discussions**

##### **3.3.1 FESEM microscopic analysis**

Electroless Ni-B coatings show nodular or cauliflower-like structures on the top surfaces of the coating. The thickness of the diffusion layer around the crystallites forming at the location of nucleation on the substrate determines the columnar structure of the Ni-B coatings. Here, the morphologies of all eight samples for the three experimental coatings are shown in figure 10 (representative image of coated sample). The finer sub-nodules are clearly visible in sample A1. In sample A2, nodules are visible but become a little flattened, and the top surface details are not as sharp as in sample A1, whereas in sample A3, significant flattening can be observed. Here, it's a notable thing that in A1, A2, and A3, which are from experiment A, each sample's deposition time is the same, i.e., 60 minutes, but the bath condition is different as deposition time progresses each hour. Similarly, B1 shows much

finer nodules in the top surface morphology as compared to B2 and B3. In B3, top surface flattening has occurred, but bigger nodules are formed because of increased deposition time. Here in samples B1, B2, and B3, deposition times are different, and bath conditions also change for each sample as deposition progresses. Refer figure 20 for experiments A & B top-surface morphology.

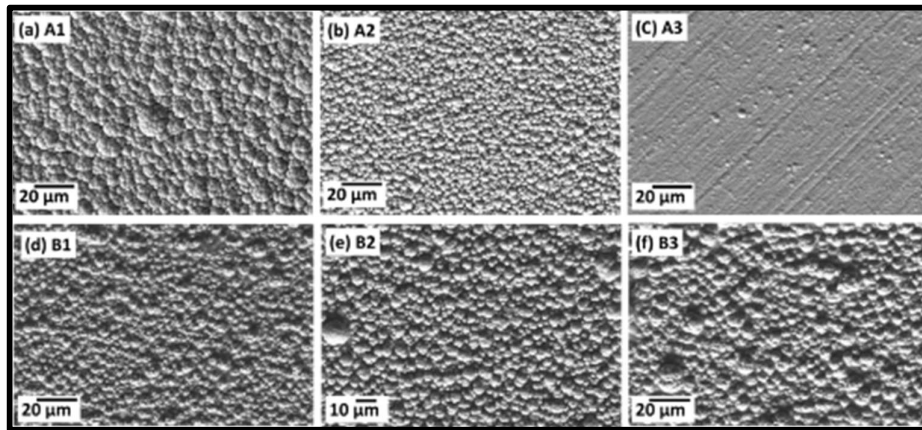


*Figure 21 Top Surface morphology of the Ni-B coating- Experiment A & B*

In both the experiments A and B, replenishment of reducing agent sodium borohydride and stabilizer lead nitrite has been done. Experiment C also shows a similar phenomenon (refer figure 21); it can be observed in C1 and C2, with significant flattening of top surface morphology in C2 as compared to C1.

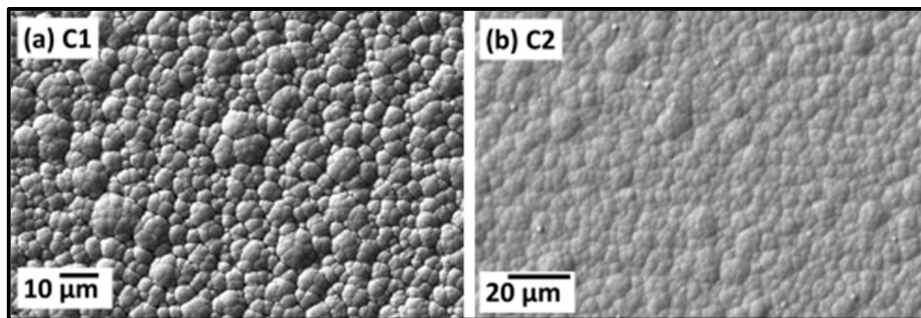


*Figure 22 Top Surface morphology of the Ni-B coating- Experiment C*

It is interesting to understand by observing all three experiments on top-surface morphology that the variations in surface morphology and microstructure can be correlated with the specific conditions of the electroless plating bath, such as pH, temperature,

and concentrations of reactants. The observed microstructural features can be related to the elemental analysis, mechanical, tribological, and corrosion-resistant properties of the Ni-B coating. The cross-section of the coating shows that it is well adherent to the substrates, refer the figure 22 where it a representative image showed.

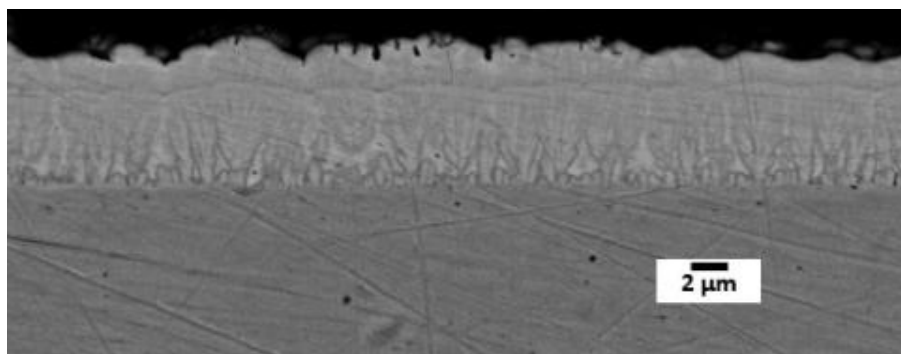


*Figure 23 Representative FESEM cross-sectional image of Ni-B coatings from experiments.*

### **3.3.2 Coating thickness analysis & pH monitoring of the bath solution**

Cross-sectional imaging can reveal the uniformity of the coating thickness and any layering effects due to deposition dynamics. Trends of thickness variation also follow the condition of bath solutions over the passage of time. With periodic bath replenishment (reducing agent and stabilizer) of bath solution, there is a drastic reduction in coating thickness observed in experiment A. A1 achieved the highest thickness, while A2 and A3 dropped significantly. Figure 23 - taken from optical microscope (OLYMPUS, U-MSSPG, TOKYO, JAPAN).

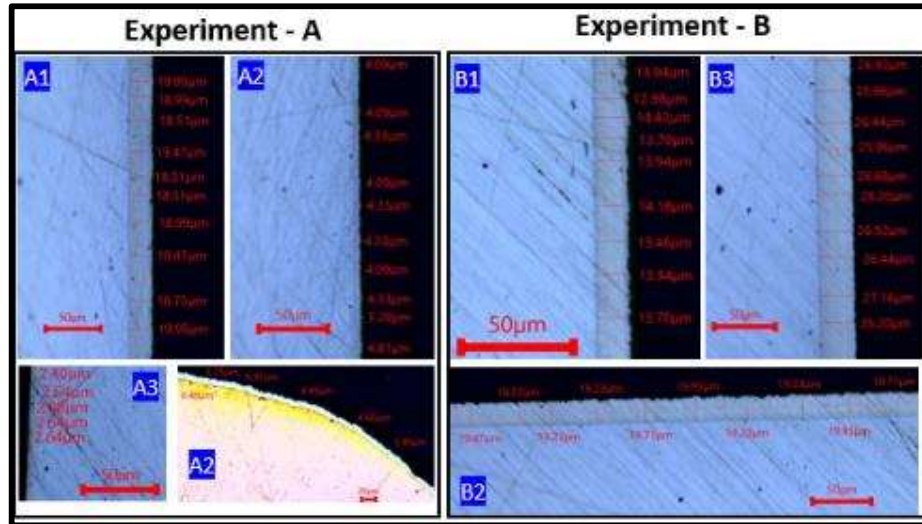


Figure 24 Cross sectional images of Experiments A & B

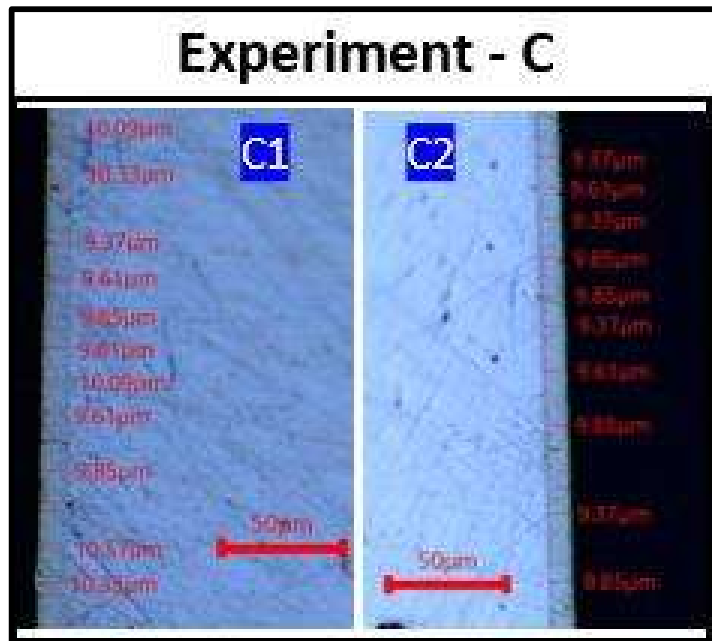


Figure 25 Cross sectional image of Experiment C

In experiment B, the periodic gain in sample thickness value gradually decreased over the duration of deposition time. With the first bath replenishment, around 6 µm of thickness was gained. So, the periodic gain in B2 is around 6 µm over B1. Similarly, for B3, the rise in thickness is around 7 µm in the last hour. It is also noticed that the deposition rates in all three experiments have

gradually reduced as deposition progresses and the coating bath gets older.

Interestingly, in experiment C, the difference in coating thickness deposited in 3 hours (sample C2) is  $9.6 \mu\text{m}$  and in the first hour (sample C1) is  $9.9 \mu\text{m}$ . There was no replenishment done in this experiment, but bath replenishment is very important for effective coating deposition. As it was not done in experiment C, the deposition almost halted after 1 hour. This reduction in the coating deposition rate can be directly reflected in the top surface morphology of the coatings.

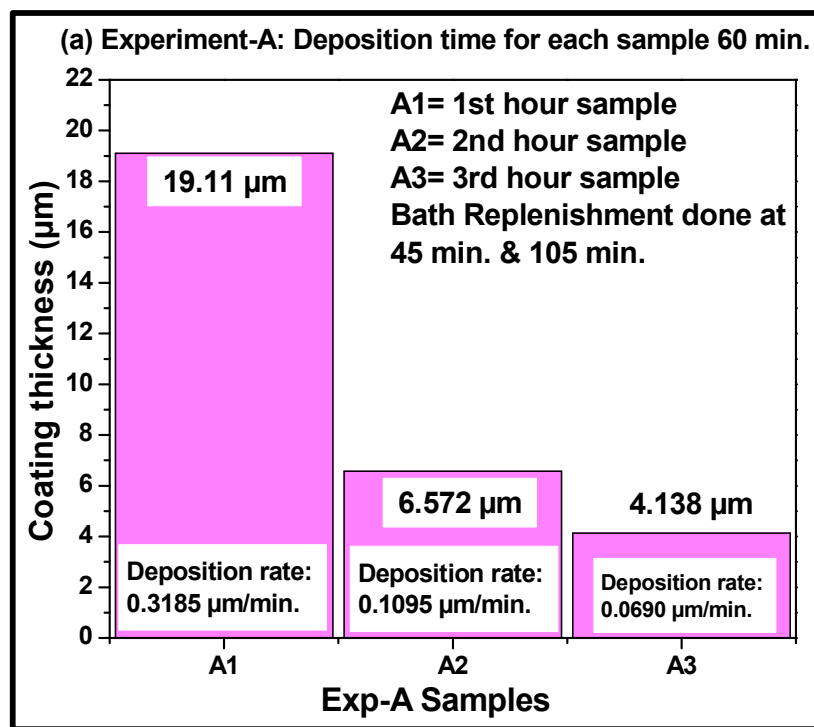


Figure 26 Experiment-A Deposition rates of samples

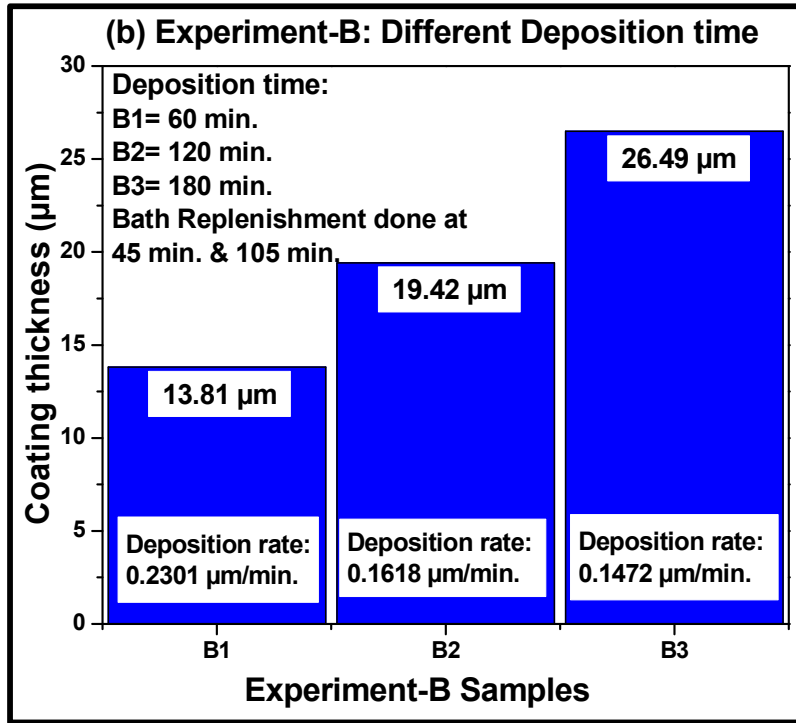


Figure 27 Experiment-B Deposition rates of samples

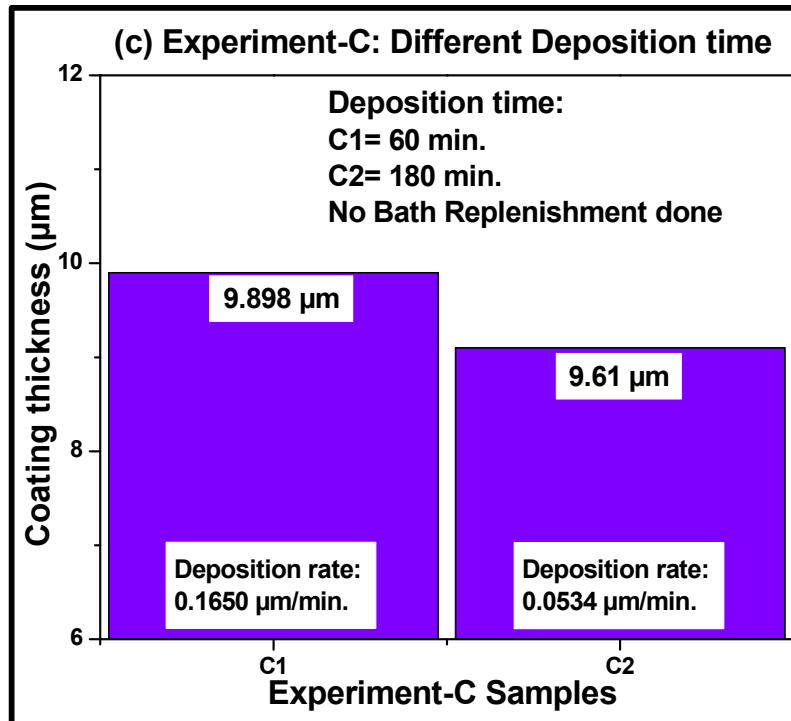


Figure 28 Experiment-C Deposition rates of samples

The standard pH value for the alkaline electroless Ni-B coating bath is  $13 \pm 1$ . Over the period of deposition, the pH value of the bath solution changes. Variations in pH values are shown in Figure 28. A small change in pH is known to cause a significant reduction in the coating deposition rate and improve the boron concentration in the deposited layers [20]. A drop in pH can affect the deposition process and the quality of the coating. It can lead to unfavorable chemical reactions like hydrolysis, which involves splitting water molecules into hydrogen ions ( $H^+$ ) and hydroxide ions ( $OH^-$ ). At lower pH,  $OH^-$  ions' concentration reduces, but the  $H^+$  ions get increased, which results in more hydrogen gas coming out of the coating bath, which will affect the coating's quality by inducing porosity. These excess hydrogen ions ( $H^+$ ) can react with other ions in the bath, such as borate ions ( $BH_4^-$ ), and form insoluble species like boric acid. These insoluble species can precipitate out and deposit on the coating surface, which will result in a rougher top surface. Figure 28 shows the pH values monitored every 30 minutes in all three experiments. With the progress of coating deposition in each bath, minor reductions in pH values have been noticed.

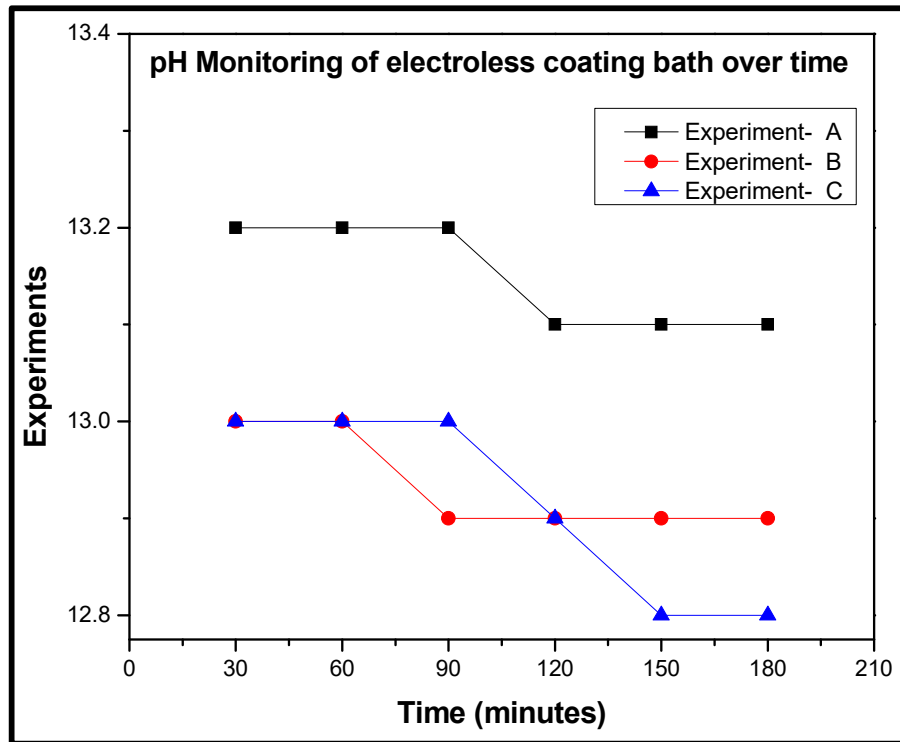


Figure 29 pH monitoring of all three experiments

### 3.3.3 ICP-AES analysis

As explained in Chapter 2, ICP-AES (inductive coupled plasma atomic emission spectroscopy) provides the elemental composition of the coating. All eight samples of coating flakes were dissolved in aqua regia to prepare the ICP-AES test samples. The elemental composition of the as-deposited electroless Ni-B coatings for all eight samples of the three experiments was determined using ICP-AES. Table 4 summarizes the concentrations of nickel (Ni) and boron (B) in the coatings.

Samples→ Elements ↓ (wt%)	Experiment- A			Experiment- B			Experiment- C	
	A1	A2	A3	B1	B2	B3	C1	C2
<b>Ni (Nickel)</b>	97.29	95.13	93.00	96.96	95.23	93.16	92.71	92.75
<b>B (Boron)</b>	2.45	4.70	6.88	2.90	4.40	6.36	6.64	7.05
<b>Pb (Lead)</b>	0.26	0.16	0.13	0.14	0.37	0.48	0.65	0.70

Table 4 Chemical composition of Ni-B coatings by ICP-AES analysis

The results indicate that the nickel content in the coatings ranges from 92.71 wt% to 97.29 wt%, while the boron content ranges from 2.45 wt% to 7.05 wt%. The variation in composition suggests some differences in the deposition conditions or bath chemistry for the different samples.

The ICP-AES analysis provided valuable insights into the elemental composition of the electroless Ni-B coatings. The nickel content was consistently high across all samples, with a slight variation, which is typical for electroless plating processes due to minor fluctuations in bath chemistry and operating conditions in these three experiments.

The boron content was found to vary more significantly, ranging from 2.45 wt% to 7.05 wt%. This variation can impact the mechanical properties of the coatings. For instance, in experiment A, sample A3 has the highest boron content (6.88%); in experiment B, sample B3 has the highest boron content (wt% 6.36); and in experiment C, sample C2 has the highest boron content (7.05 wt%). This increase in boron wt% can occur due to the significant reduction in coating deposition rate. The coating deposition rate is decreasing as the deposition is occurring, and the pH value has decreased slightly [20].

The observed compositional variations could be attributed to several factors, including:

- a. **Bath Composition and different sample deposition condition:** There might be differences in the concentration of

the reducing agent (sodium borohydride) or stabilizers in the plating bath in each experiment or it can also depend on the deposition conditions of the samples.

- b. **Deposition Parameters:** Variations in temperature, pH, and deposition time can influence the rate of nickel and boron co-deposition. Here, a slight variation in pH has occurred as deposition progresses.
- c. **Bath Aging:** The age and usage history of the plating bath, which can alter the effective concentrations of reactants over time. A rise in the boron content is observed in samples undergoing longer duration of deposition.

To further understand the impact of these variations, additional studies on the microstructure, phase composition, and mechanical properties of the coatings are necessary. X-ray diffraction (XRD) and hardness testing can complement the ICP-AES data, providing a comprehensive understanding of how elemental composition influences the overall performance of electroless Ni-B coatings.

#### 3.3.4 XRD analysis

In the XRD analysis, the XRD data was obtained for the electroless Ni-B coatings of all three experiments (A, B, and C). Here are figures 29, 30 and 31, to display the diffraction patterns and the identified phases.

The broadened peaks of Ni (111) observed  $44.5^\circ$  ( $2\theta$ ) indicate the existence of both microcrystalline and amorphous phases [24, 25].

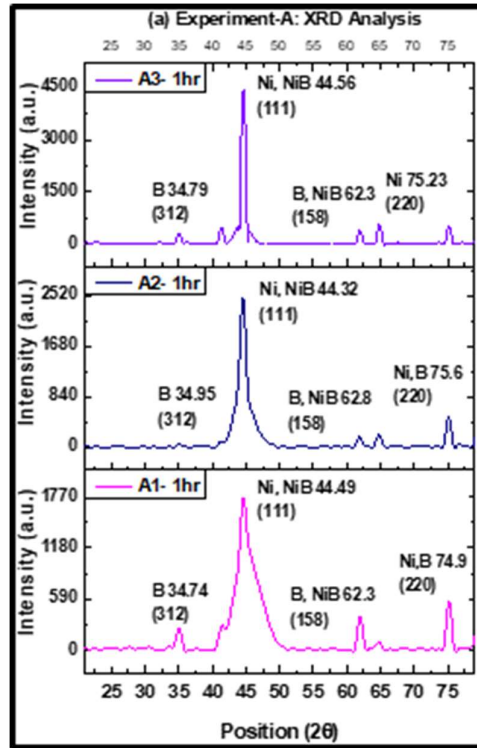


Figure 30 XRD Analysis for experiment A

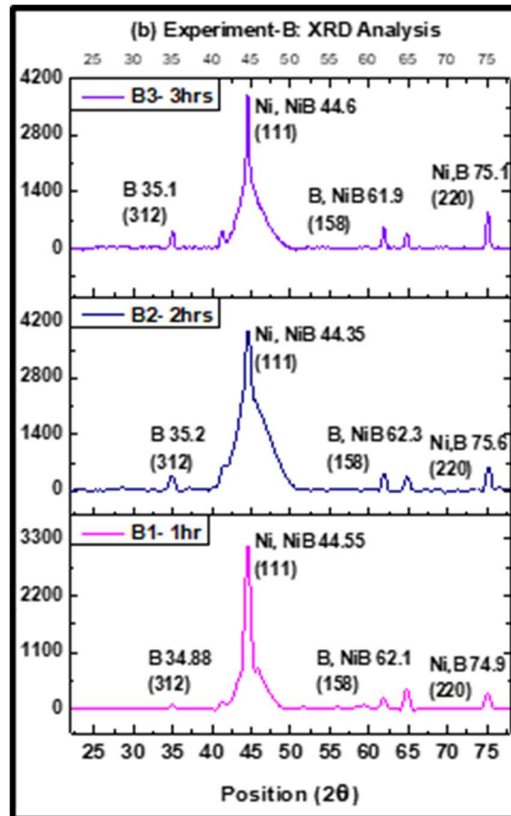


Figure 31 XRD Analysis for experiment B

This amorphous and crystalline structure in the Ni-B coatings reveals the role of boron in governing the deposition mechanism by restricting nickel's nucleation and hence restraining crystallization [17, 26, 27]. In the XRD graph, it is observed that the boron is present around 35°, and at 62°, the Ni-B phase is also present.

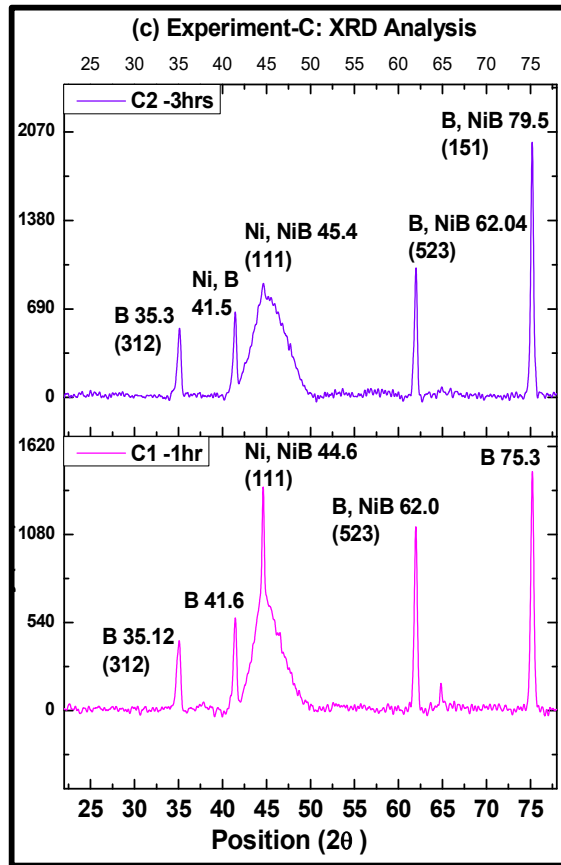


Figure 32 XRD Analysis for experiment C

The sharp and well-defined peaks in the XRD patterns indicate a high degree of crystallinity in the electroless Ni-B coatings. High crystallinity is often associated with improved mechanical properties, such as increased hardness and wear resistance. In this study for experiments A, B, and C, crystallinity is increasing as deposition progresses (or bath is getting older).

In this section, we present the results of the Williamson-Hall analysis used to determine the crystal size and lattice strain in the electroless Ni-B coatings. Below table 5 and figure 32 show the

crystal size calculation by the Williamson-Hall and Scherrer formulas.

The Williamson-Hall (W-H) method was used to estimate the crystal size and lattice strain of the electroless Ni-B coatings. The W-H equation is given by:

$$\frac{\beta r \cos\vartheta}{k\lambda} = \frac{1}{L} + \frac{4e \sin\vartheta}{k\lambda}$$

Where:

$\beta r$  → Integral breadth of the peak

$\lambda$  → Wavelength of X-ray radiation (0.15418nm) Cu scan

L → Avg. crystallite size

$\theta$  → Bragg angle

K → constant, 0.9

e → lattice strain in the material

The FWHM ( $\beta$ ) and Bragg angles ( $\theta$ ) for the prominent diffraction peaks were determined from the XRD patterns [21, 22].

Sample	Crystal size by Williamson Hall	Crystal size by Scherrer formula	Coating Bath freshness
A1	8.553803	10.12	First- 60 minutes
A2	14.45424	12.4	Started after 60 minutes
A3	15.24635	12.50	Started after 120 minutes
B1	13.41612	13.42	First- 60 minutes
B2	14.26334	14.00	120 minutes older bath
B3	14.9793	20.95	Removed in 180 minutes
C1	12.27988	22.58	First- 60 minutes
C2	13.62614	22.44	Removed in 180 minutes

Table 5 Crystal size is calculated by Williamson Hall calculation and Scherrer

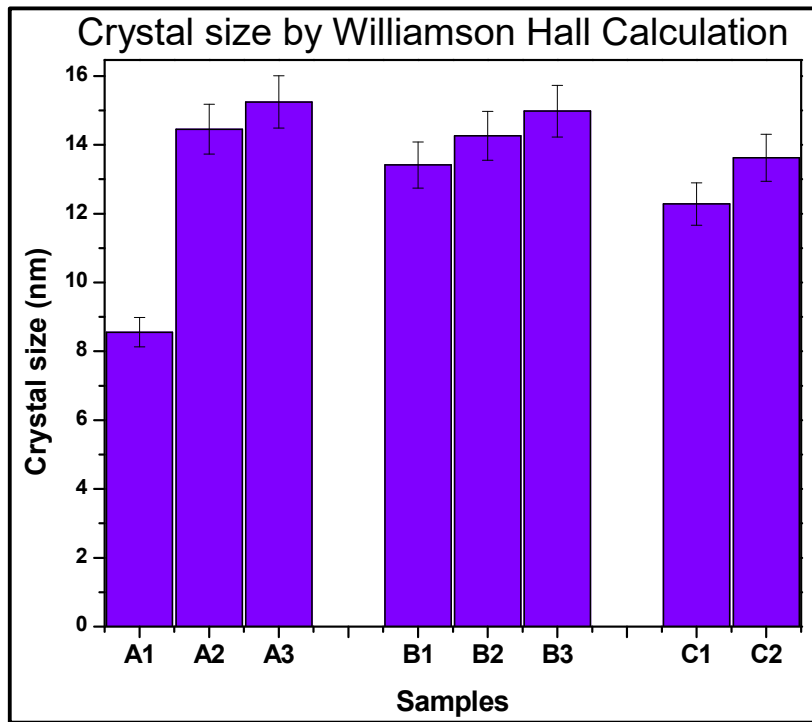


Figure 33 Crystallite size by Williamson-Hall calculation for experiments A, B & C

The Williamson-Hall analysis of the electroless Ni-B coatings has given an understanding of the microstructural properties. The nanocrystalline structure and low lattice strain are indicative of high-quality coatings with excellent mechanical properties. These findings, combined with the ICP-AES and XRD results, offer a comprehensive view of the coating's composition and performance, guiding further optimization of the electroless plating process for various industrial applications.

The Scherrer formula assumes particles have equal dimensions in all directions (equiaxed), while the Williamson-Hall method accounts for both equiaxed and un-equiaxed particles (with different dimensions in different directions). Consequently, the Williamson-Hall method provides information on both crystallite size and strain broadening, making it more effective than the Scherrer formula.

### 3.3.5 EDS analysis

The EDS analysis was conducted to determine the elemental composition of the electroless Ni-B coatings. Figure 33 shows the EDS spectrum for a representative sample from the three experiments, and Table 6 summarizes the quantitative elemental composition of eight different samples from experiments A, B, and C, where nickel, boron, carbon, and a low amount of oxygen are present in all the samples except A3 and C1.

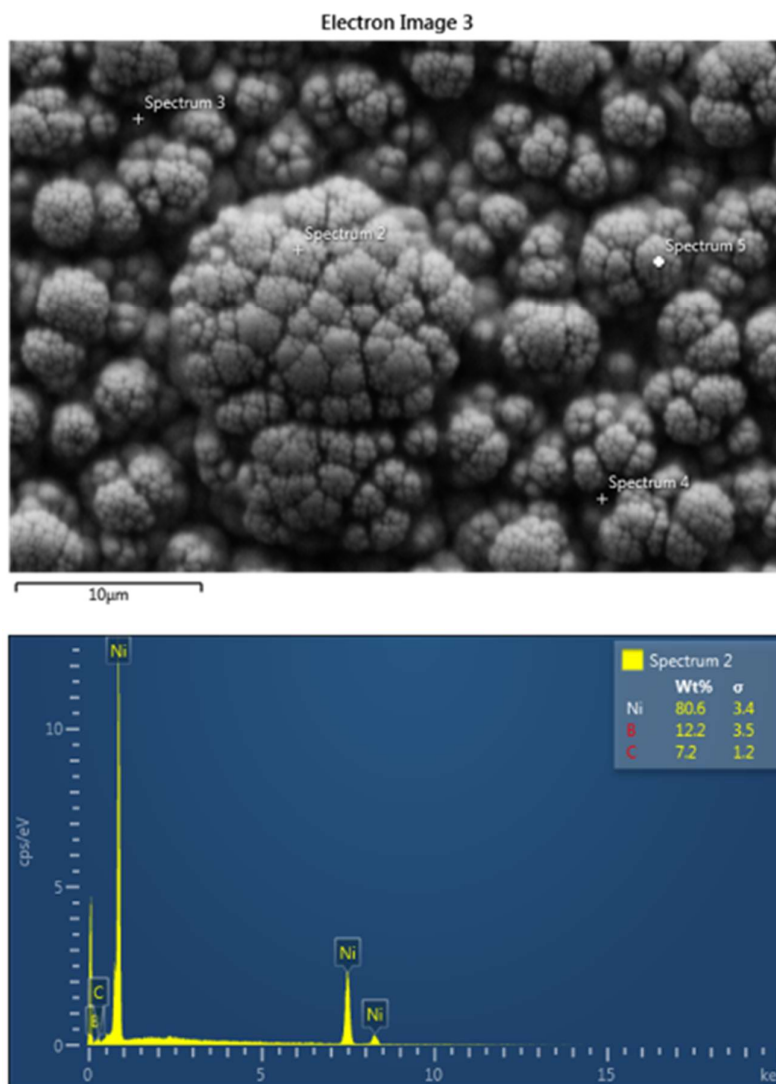


Figure 34 Representative image of EDS analysis of the experiments

Samples→	Exp- A			Exp- B			Exp- C	
	A1	A2	A3	B1	B2	B3	C1	C2
Elements↓								
Ni	79.98	74.28	80.2	74.51	76.49	74.49	81.12	80.6
B	9.45	13.17	7.5	13.63	11.85	13.02	9.0	5.1
C	<b>6.82</b>	<b>8.11</b>	<b>12.3</b>	<b>7.90</b>	<b>8.28</b>	<b>8.48</b>	<b>9.8</b>	<b>10.9</b>
O	3.75	4.45	-	3.96	3.38	4.01	-	3.4

Table 6 Elemental Composition of Electroless Ni-B Coatings from Experiments A, B&C

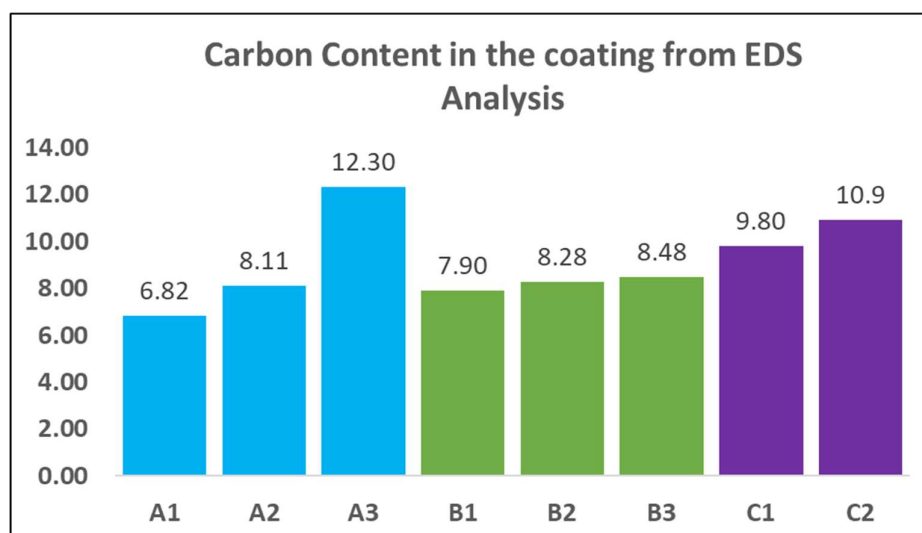


Figure 35 Carbon wt% of all three experiments from EDS analysis

Elemental Composition of observed as follows:

1. **Nickel (Ni):** Nickel is the predominant element in the coatings, with concentrations ranging from 74.28 at% to 81.12 wt%. This high nickel content is expected as it forms the primary matrix of the Ni-B coating.
2. **Boron (B):** The boron content varies slightly between samples as deposition progresses, ranging from 7.9 wt% to 12.3 wt%. Boron content varies slightly, likely due to minor differences in deposition conditions.

3. **Carbon (C):**The concentration of carbon in the coating ranges approximately from 8.28 wt% to 12.3 wt%. This carbon comes from the chemical reactions happening in the bath solution. Refer to figure 34 for carbon wt% in all experiments.
4. **Oxygen (O):**The presence of oxygen in all samples, ranging from 3.4 to 4.0 wt%, is likely due to surface oxidation. This is common for electroless coatings exposed to air and does not significantly affect the bulk properties of the coating.

Among these three experiments (A, B, and C), the carbon percentage shows distinct variation with respect to the time of deposition. As the plating bath grows older, more carbon gets incorporated into the matrix of the deposited layer. With that, the effect of such variations in boron and carbon in the coating needs to be investigated. The incorporation of different concentrations of carbon in the electroless Ni-B coatings may affect the structural formation of the coating.

Carbon nanotubes can also act as nucleation sites for the growth of Ni-B grains during deposition of coatings, so the concentration of carbon may result in the change in grain size, which can further influence in the mechanical properties of the coatings. [29].

### 3.3.6 Raman Spectroscopy

Raman spectroscopy was used to evaluate the structural changes in electroless Ni-B coatings deposited over varying deposition times and bath conditions in different experiment samples. This analysis aimed to assess the influence of deposition time and bath conditions on the formation of coating phases related to any carbon-related structures. Figure 35 illustrates the Raman spectra for these experiments, highlighting key peaks, including those associated with carbon, times & bath conditions [23].

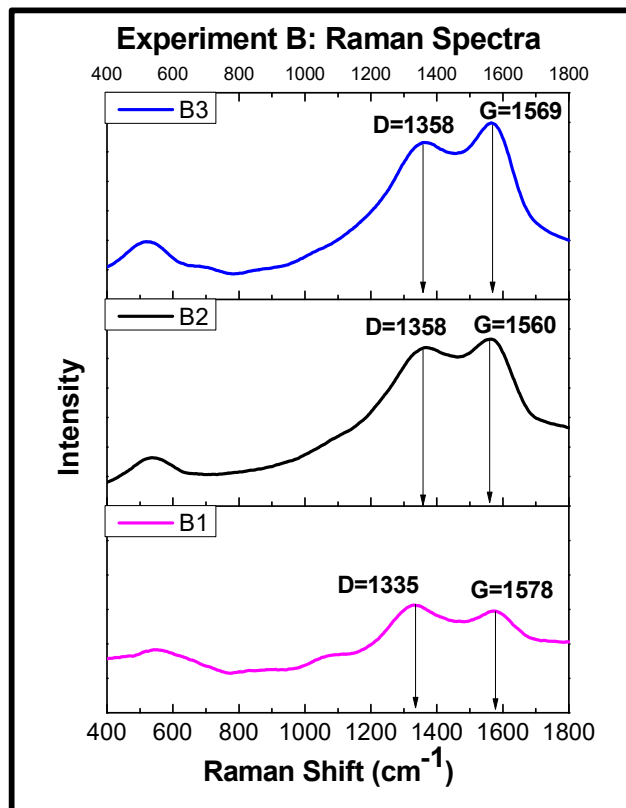
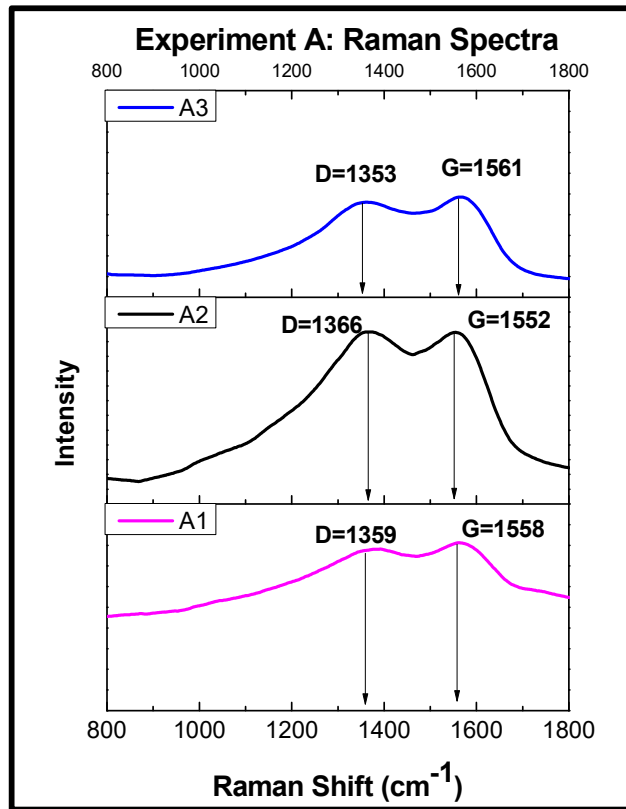


Figure 36 Raman Spectra of Electroless Ni-B Coatings with Different Deposition

Experiments	Bath freshness age (in minutes)	Raman Shift (cm <sup>-1</sup> )	Assigned Vibrations
Exp-A (each sample deposition time 60 Min.)	A1 (60Min.)	1359, 1558	D-band, G-band
	A2 (120Min.)	1366, 1552	D-band, G-band
	A3 (180Min.)	1353, 1561	D-band, G-band
Exp-B (Deposition time B1- 60min., B2-120min. & B3-180min.)	B1 (60Min.)	1335, 1578	D-band, G-band
	B2 (120Min.)	1358, 1560	D-band, G-band
	B3 (180Min.)	1358, 1569	D-band, G-band

Table 7 Carbon D & G band raman shift for each samples

The Raman spectroscopy analysis provides insight into the structural and compositional evolution of electroless Ni-B coatings over different deposition times. Key findings include consistent Ni-B bonding and evidence of surface oxidation, as well as the presence of carbon structures, represented by the D and G bands. Carbon-related peaks at 1350 cm<sup>-1</sup> (D-band) and 1600 cm<sup>-1</sup> (G-band) indicate the presence of disordered (amorphous) and graphitic carbon, respectively. These carbon structures may arise from organic contaminants or decomposition products from the plating solution.

The identification of carbon within the Ni-B matrix opens up potential for tailored functionalities, such as modified frictional behavior or enhanced thermal stability, important for advanced engineering applications.

### 3.3.7 XPS analysis

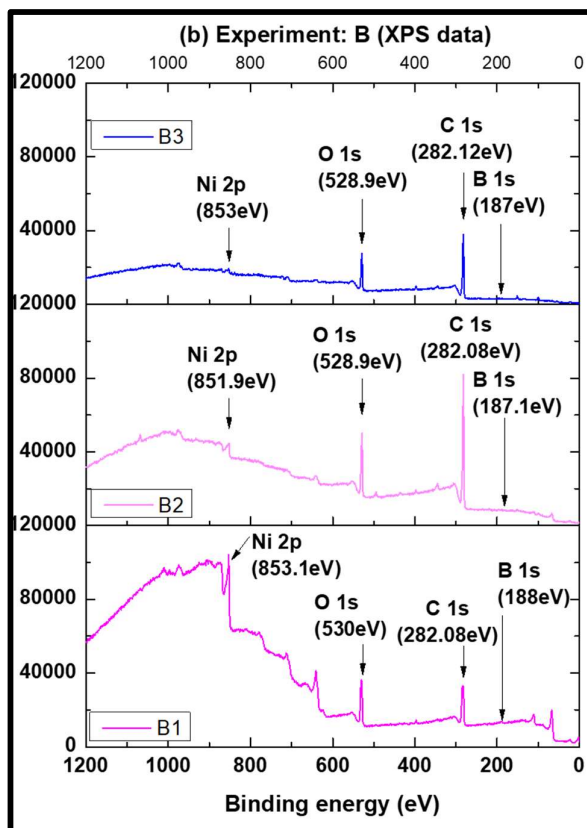
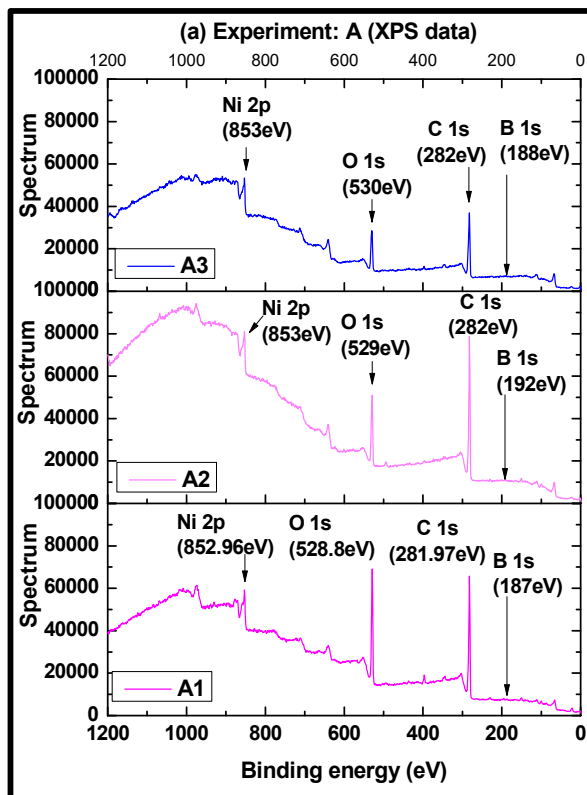
X-ray Photoelectron Spectroscopy (XPS) was performed on electroless Ni-B coatings deposited over three different time deposition and bath conditions (experiments A, B, and C). This analysis was to understand the chemical state and elemental composition of the surface layers of the coatings. Key findings include shifts in binding energies and variations in elemental ratios as a function of deposition time and bath condition as coating deposition progresses. Table 8 shows the binding energy of the elements for all the samples.

The Ni 2p spectra for all samples show a narrow two sub-peaks at 853eV (doublet peak) typical of nickel compounds, with slight shifts in binding energy indicating changes in the nickel's chemical environment due to varying boron content and possible oxidation.

<b>Experiments</b>	<b>Bath freshness age (in minutes)</b>	<b>Binding Energy (eV)</b>	<b>Element</b>
Exp-A (each sample deposition time 60 Min.)	A1 (60Min.)	852.96; 187; 281.97	Ni 2p; B1s; C1s
	A2 (120Min.)	853; 192; 282	Ni 2p; B1s; C1s
	A3 (180Min.)	853; 188; 282	Ni 2p; B1s; C1s
Exp-B (Deposition time: B1- 60min., B2- 120min. & B3- 180min.)	B1 (60Min.)	853.1; 188; 282.1	Ni 2p; B1s; C1s
	B2 (120Min.)	851.9; 187.1; 282.1	Ni 2p; B1s; C1s
	B3 (180Min.)	853; 187; 282.1	Ni 2p; B1s; C1s
Exp-C (Deposition time: C1- 60min. & C2- 180min.) Without bath replenishment	C1 (60Min.)	853; 185; 282	
	C2 (180Min.)	852.1; 188; 282	

*Table 8 Key Binding Energies and Elemental Ratios for Electroless Ni-B Coatings*

Figure 36 shows XPS analysis of all the three experiments with elemental binding energy.



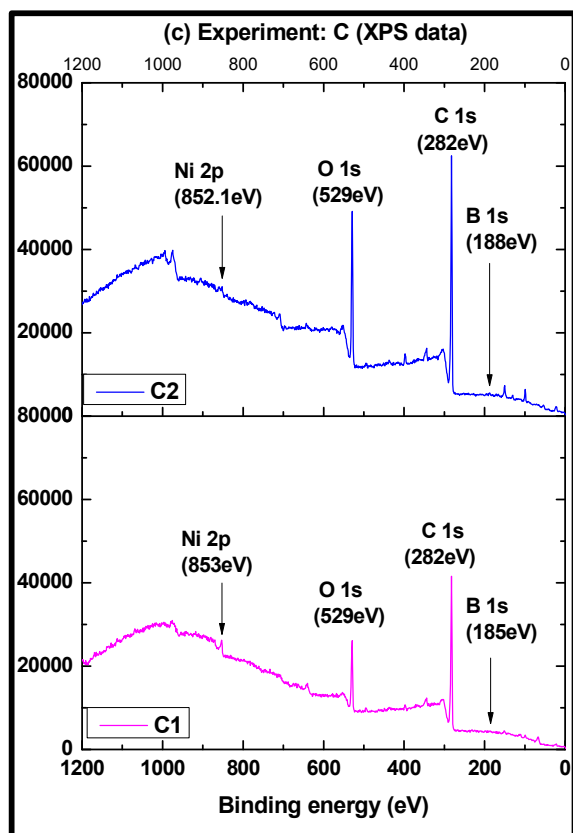


Figure 37 XPS Spectra of Electroless Ni-B Coatings with Different Deposition conditions

B 1s peaks indicate boron's incorporation into the nickel matrix, consistent with the formation of Ni-B alloys. The slight increase in binding energy across deposition times could suggest changes in the boron environment, potentially indicating a denser or more complex boron integration within the matrix as deposition time increases. Here, the C1s peak indicates carbon's peak in the Ni-B coatings, but to accurately determine the nature (or compound) of the carbon present here and its implications for the properties of the coating, comparing the XPS results with other characterization methods such as Raman spectroscopy, which can confirm the presence and form of carbon, is beneficial. In Section 3.3.6, the D and G bands of carbon are found at approximately 1358 and 1560  $\text{cm}^{-1}$  Raman shifts. The G-band carbon atoms, typically found in graphitic materials, indicate graphitic carbon, whereas the D-band is generally activated by defects or disorders within the graphitic

structure. This band is not present in perfect graphite and indicates structural imperfections or edges. The presence of both D and G bands suggest that carbon in the electroless Ni-B coatings is predominantly in the form of disordered graphite or amorphous carbon.

XPS analyses of coatings show the presence of carbon at the top surface of the coatings and that may be attributed to the presence of a carbon containing constituent in an electroless solution, such as the complexing agent Ethylenediamine (EDA,  $C_2H_8N_2$ ). In case, a longer duration of deposition is performed to achieve a thicker coating, this carbon may get adsorbed at the top surface of coatings. It should be noted that the X-ray photoelectron spectroscopy (XPS) is a surface-sensitive quantitative spectroscopic technique. With a standard sampling depth 0–20 nm in XPS [30, 31, 32], it can be ascertained that carbon peak identified in the analysis is detected only from the top layer of (a few nanometers) the coating. With the top layer of deposits being the dominant inhabitation of carbon, all other phases and their respective properties remain unaffected. However, in the case of electroless coating where carbon is mainly present as contamination because of dissociation of the constituents of a bath solution if it is not visible in XRD pattern. Meanwhile, coatings containing carbon-based reinforcing phases show sharp peak of carbon in XRD analysis [33-34].

### **3.4 Mechanical and tribological characterization**

#### **Introduction**

In this chapter, physical characterization and elemental analysis results have been discussed in brief, and now in this section, mechanical and tribological analysis such as microhardness (Vickers), scratch tests, and sliding wear tests at room temperature have been discussed.

### 3.4.1 Result and discussion

#### 3.4.1.1 Vickers Microhardness test

The Vickers microhardness test was conducted on the cross-sectional area of the Ni-B electroless coatings deposited on a steel substrate for all three experiments, except for samples A2 and A3 because of their lower thickness, so the hardness is verified by taking compound hardness; refer to figure 38 for compound hardness and figure 37 for cross-sectional hardness. The hardness of a composite coating depends on the phases present in its matrix. There are 10 points considered to calculate average hardness.

Experiments	Sample#	Micro hardness at cross section (at Hv <sub>0.03</sub> )
Exp-A (each sample deposition time 60 Min.)	A1 (60Min.)	753.8
	A2 (120Min.)	Cross section thickness less
	A3 (180Min.)	Cross section thickness less
Exp-B (Deposition time: B1-60min., B2-120min. & B3-180min.)	B1 (60Min.)	788.2
	B2 (120Min.)	799.8
	B3 (180Min.)	779.9
Exp-C (Deposition time: C1-60min. & C2-180min.)	C1 (60Min.)	732.2
	C2 (180Min.)	736.9

Table 9 Cross section micro hardness at Hv<sub>0.03</sub> load (30gram load).

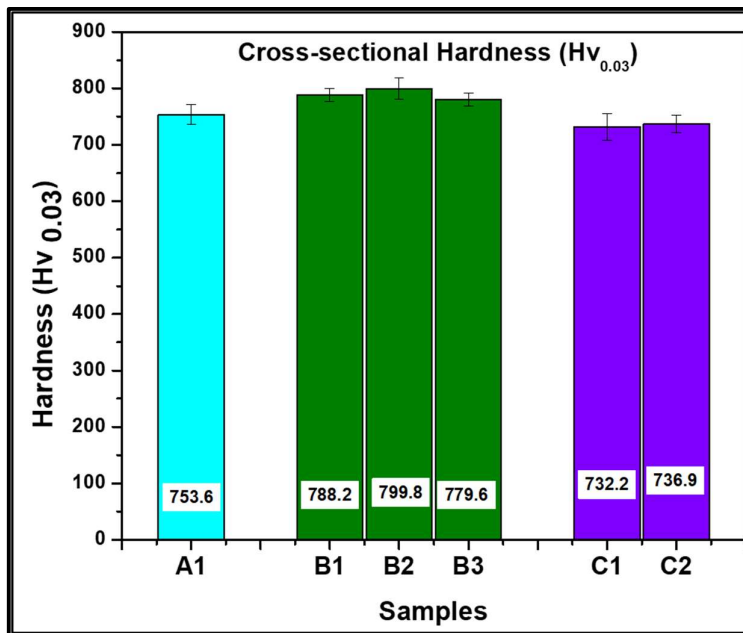


Figure 38 Cross section micro hardness at Hv<sub>0.03</sub> load

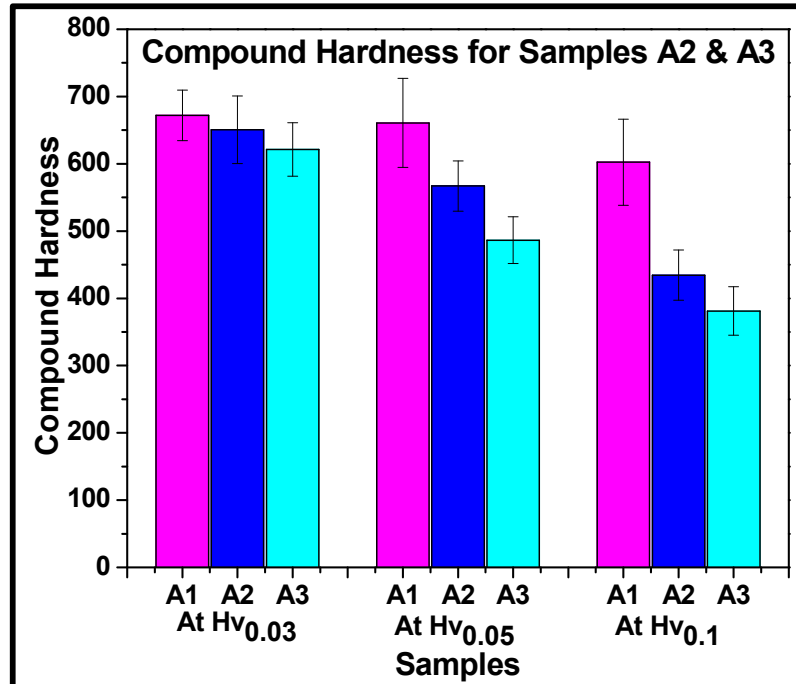


Figure 39 compound hardness of experiment A samples to compare hardness of A2 and A3 at 30, 50, and 100-gram load

In experiment B there the deposition time for sample B1 was 60 minutes, B2 was 120 minutes and B3 was 180 minutes, microhardness observed 788.2  $Hv_{0.03}$ , 799.8  $Hv_{0.03}$ , & 779.9  $Hv_{0.03}$  respectively. Here it is noticeable that the B1 & B2 Hardness are increasing as the boron wt% are increasing in the coating but decreased in B3 though the boron wt% increased. It happened because the carbon inclusion here is not supporting the mechanical properties, as this carbon inclusion was identified from EDS and XPS analysis and confirmed by Raman spectroscopy that there are G and D bands of graphite or amorphous carbon available. This amorphous carbon is present in the coating in a disordered manner at the grain boundaries, which results in structural imperfection. So, this little variation is coming from this amorphous carbon. Whereas in experiment C there is not much difference, C1 hardness observed 732.2  $Hv_{0.03}$  and C2 is 736.9  $Hv_{0.03}$  in hardness because the coating deposition is stopped as there was no bath replenishment done.

### 3.4.1.2 Scratch tests

The scratch test was conducted on the top surface of Ni-B electroless coatings deposited on steel substrates. The objective was to evaluate the coating's adhesion strength, scratch resistance, and failure mechanisms. Scratch tests are performed three times on each sample to ensure consistency in the scratch test. There are three experiments and eight samples performed for a scratch test as per the process parameters listed in Table 10.

Parameters of scratch testing	
Scratch length	3mm
Scratch load	10N
Scratch speed	0.1mm/sec

Table 10 Scratch test parameters at RT

Coefficient of friction (COF) graphs of exp. A, B & C are shown in figure 39, 40 & 41

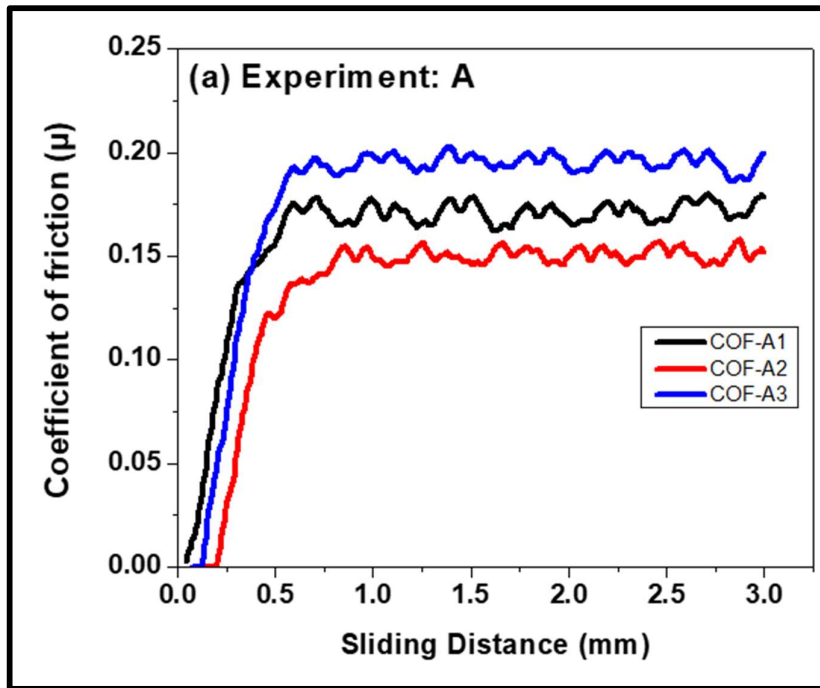


Figure 40 Scratch test- COF for Experiment A samples

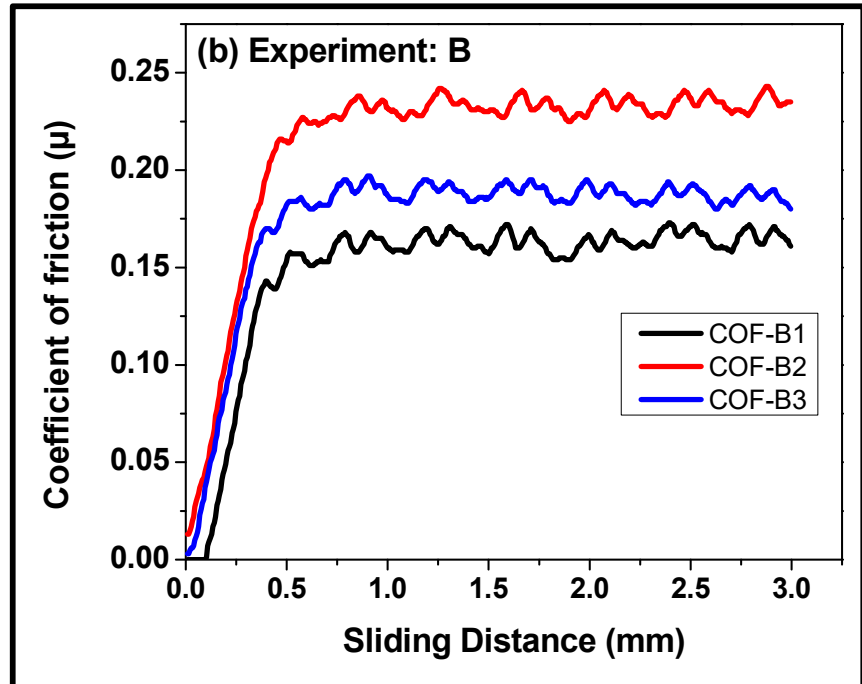


Figure 41 Scratch test- COF for Experiment B samples

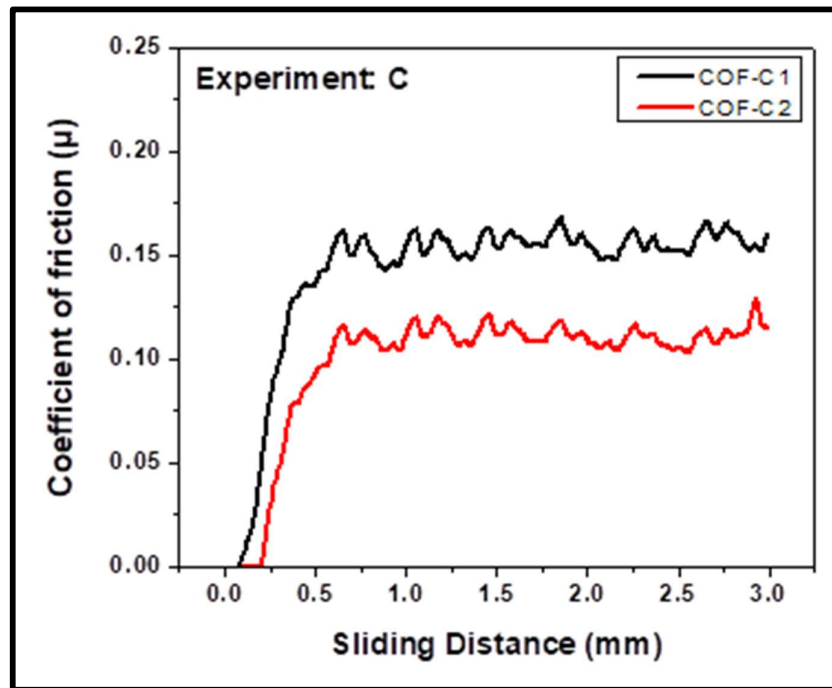


Figure 42 Scratch test- COF for Experiment C samples

Scratch hardness is also identified as lateral hardness, and it reflects the coating's resistance to plastic deformation in a quasi-

static lateral indentation (Guilherme et al., 2018). The scratch hardness of all eight samples is shown in figure 42 with the calculation of a 10N scratch load. In this experiment A, the scratch hardness of A3 (3.2 GPa) is greater than that of A2 (2.8 GPa), which is due to the inclusion of more boron. There are various factors, such as deposition time, coating thickness, boron inclusion, and amorphous carbon (or graphite), that affect the scratch hardness trend, which have been verified with different characterization methods.

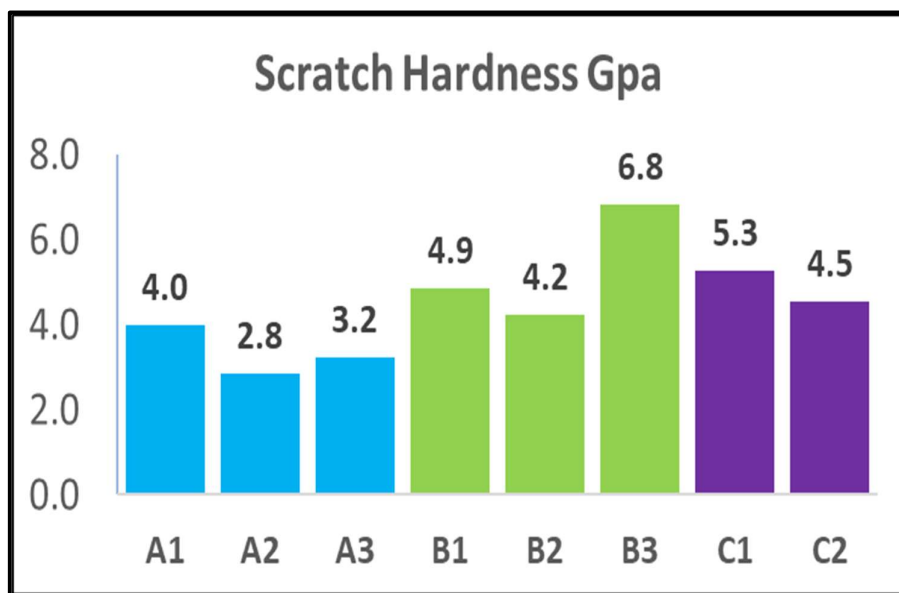


Figure 43 Scratch hardness for all eight samples

### 3.4.1.3 Sliding wear tests

The tribological performances of all developed coatings are studied under the dry reciprocating wear test, and the and the sliding wear test parameters are shown in Table 11. The trend of the coefficient of friction is displayed in figure 43 for all eight samples.

In experiment A, the COFs of A1, A2, and A3 are 0.44, 0.38, and 0.39, respectively. But the hardness trend seems counterintuitive

in such conditions where the COF is higher and the hardness is also high. It can happen because A2 and A3 have less thickness, and the deposition conditions are different for each sample. As the deposition takes place, the bath conditions also change, and it is also observed in the top surface morphology that significant flattening occurs as deposition takes place.

Parameters of Sliding Wear Test	
Amplitude	3mm
load	3N
Frequency	20Hz
Time	15 Min.

Table 11 Sliding wear test parameters

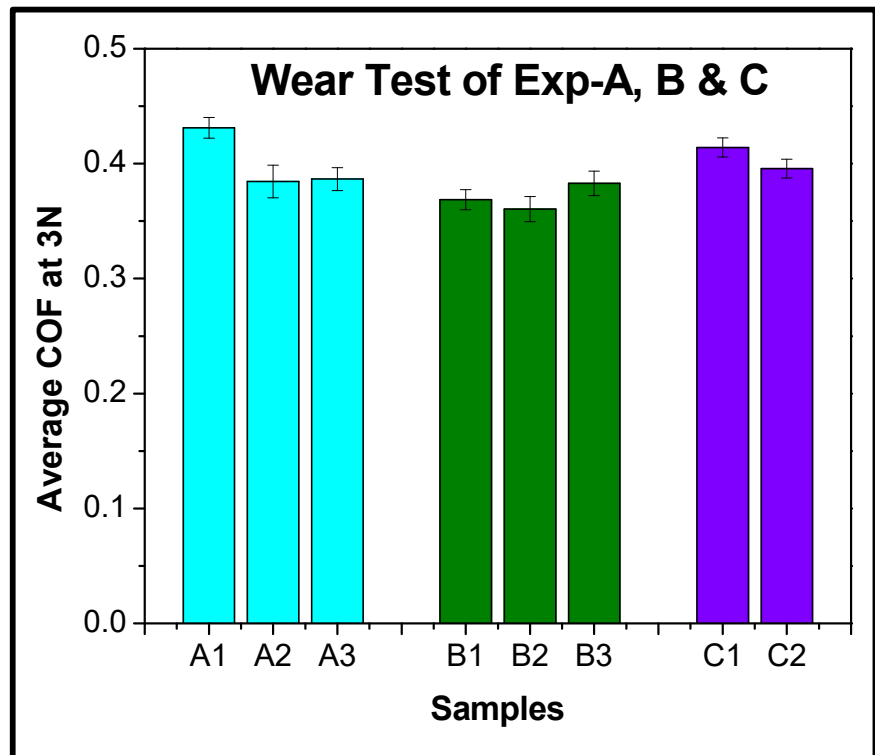


Figure 44 Wear test- AVG. COF for experiments A, B & C

Coating's cohesive strength is probably reduced because of the amorphous carbon. They act in a similar manner to that happens in a cast product having defects created by the inclusion of oxides or molding impurities. A material with lack of cohesive strength displays higher value of COF.

## CHAPTER 4

### **Overall conclusions and future work scope**

---

#### **4.1 Introduction**

Electroless Ni-B alloy coatings are successfully fabricated and deposited onto the AISI 1025 substrates in all three experiments. In chapter 3, the development of electroless coatings Ni-B with different deposition conditions is explained with all the characterizations such as top surface and cross-sectional morphology by FESEM, EDS, XRD, ICP-AES, Raman spectroscopy, XPS, microhardness, and tribological tests in detail. Now, in this chapter, a conclusion to the whole chapter is drawn and future scope is discussed.

#### **4.2 Conclusions**

- Electroless Ni-B coating is successfully deposited onto the low-carbon steel substrate AISI 1025 with three different deposition times and bath conditions, with and without bath replenishment.
- The top surface morphology reveals a cauliflower-like structure observed under FESEM, as deposited Ni-B coatings also show the ability of retaining the lubricants due to its columnar and nodular structure under the adhesive wear conditions [10]. Formation of this cauliflower-like morphology at the top surface can be related to the columnar growth structure of the coating proceeding through nano-grains' nucleation. Here, the chemical bath produces multitude of nucleation points at isolated zones, favorably at peaks or valleys of the surface profile of the substrate and then the growth progresses to lateral directions and forms a smooth continuous film [17, 19].

The cross-sectional image that the coating is well adherent to the substrates. The finer nodules are visible in the initial 60-minute coating in all three experiments, but the 120-minute

coatings' top surface details are not as sharp as the 60-minute coatings. And in the last hour (180 minutes), significant flattening was observed.

- **Deposition rate:** The deposition rate was decreasing as deposition took place and the coating bath got older. Whereas in experiment C, where bath replenishment is not done, the deposition was halted after one hour, and the reduction in deposition rate can be directly reflected in the top surface morphology of the coating. Over the period of deposition, the pH value of the bath solution decreases, and small changes in pH can cause a significant reduction in the coating deposition layer.
- In the EDS analysis, carbon wt% shows distinct variation with respect to time of deposition. As the plating bath grows older, more carbon gets incorporated into the matrix of the deposited layer.
- XRD analyses: The deposited Ni-B coating matrices indicate a mixture of amorphous and crystalline structures. Crystallite size was calculated by the Scherrer and Williamson-hall methods for all three experiments, and it was found that as the deposition progressed, crystallite size increased because the deposition rate decreased.
- The ICP-AES analyses show that the boron content in coatings increases with a decrease in the pH value of the coating bath, and this pH is decreasing as deposition progresses and the plating bath gets older.
- XPS analyses show carbon (C1s) at 282 eV binding energy, so to accurately know the nature of this carbon, Raman spectroscopic analyses are done, and it was observed that the D and G bands of amorphous (or disordered graphite) carbon are present at 1358 and 1560  $\text{cm}^{-1}$  peaks. It is understood that the carbon has not integrated with the lattice of the coating matrix in order to positively influence coatings' mechanical properties. The longer a bath solution is used for coating

deposition with or without replenishments, the more carbon inclusions are observed. This results in a general trend of decline in microhardness. However, with the passage of time, as the deposition rate slows down with observed reduction in pH value of the bath, boron concentration increases in the coating matrix. The presence of boron and its concentration benefits hardness and tribological properties of the coating. So, the overall characteristics developed in coatings developed through the electroless route in this study bear coordinated effects of carbon and boron concentrations.

- As the electroless Ni-B coating deposition progresses, chemical reactions occur in the bath and result in the inclusion of carbon in the deposits. Concentration of carbon in deposits increases as the bath gets older.
- Amorphous carbon is not strengthening the coating, as an overall degradation in tribological properties of samples with respect to the evaluated carbon content is observed. It is possible when the carbon is amorphous and is located in between matrices instead of the lattice.

### **4.3 Scope for future work**

- In Raman spectroscopy, the D and G band peaks suggest the presence of amorphous carbon in the deposited layers. This carbon is not contributing to the strengthening, and it is very much likely that instead of being a part of the lattice, it is located in between grains. Shift in nickel peaks in the diffraction data can help in pinpointing the position. This requires further investigations.
- Various studies have demonstrated the presence of carbon in electroless Ni-B coatings; however, the impact of amorphous carbon within electroless deposition remains unexplored. Further detailed studies may give more insights into the variations in mechanical properties caused by the compositional changes developed by an aging electroless bath.

## REFERENCES

1. Shipway, P. H. and Mellor, B. G., (Ed.) (2006), The range of surface coating methods, In: Surface coatings for protection against wear, Woodhead Publishing Limited, England, e1.
2. Holmberg, K., and Matthews, A., (2009), Coatings tribology: properties, mechanisms, techniques and applications in surface engineering, Elsevier.
3. Rickerby, D. S., and Matthews, A., (1991), Advanced surface coatings: a handbook of surface engineering, Glasgow, UK, Blackie.
4. Burakowski, T., and Wierzchon, T., (1998), Surface engineering of metals: principles, equipment, technologies, CRC press.
5. Mallory, G. O., and Hajdu, J. B., (1990), Electroless plating: fundamentals and applications, American Electroplaters and Surface Finishers Society, Orlando, FL, 1-56, (ISBN: 0936569077, 9780936569079)
6. Vaibhav Nemane, MAY 2022, Vol. 144 / 051402-1, Nanomechanical, Tribological, and Scratch Properties of Electroless Ni-B-W Alloy and Ni-B-W-SiC Composite Coatings
7. Brenner, A., and Riddell, G. E., (1946), Nickel plating on steel by chemical reduction, J. Res. Natl. Bur. Stand., 37, pp. 31-34
8. Wan, Y., Yu, Y., Cao, L., Zhang, M., Gao, J., and Qi, C., (2016), Corrosion and tribological performance of PTFE-coated electroless nickel boron coatings. Surface and Coatings Technology, 307, pp. 316-323
9. Warf J. C. and Schaltegger K. H., (1955), Method of coating steel with Nickel-boron, US patent 2726170.
10. Bonin, L., Vitry, V., and Delaunois, F., (2020), Inorganic salts stabilizers effect in electroless nickel boron plating: stabilization mechanism and microstructure modification, Surf. Coat. Technol., 401, pp. 126276

11. Sudagar, J., Lian, J., and Sha, W., (2013), Electroless nickel, alloy, composite, and nano coatings-a critical review, *J. Alloys Compd.*, 571(1), pp. 83-204.
12. Agarwala RC and Agarwala V. Electroless alloy/composite coatings: a review. *Sadhana* 2003;28(3–4), pp.475–93
13. Sahoo, P., and Das, S. K., (2011), Tribology of electroless nickel coatingsA Review, *Mater. Des.*, 32(4), pp. 1760-1775
14. Delaunois, F., Petitjean, J.P., Lienard, P., Jacob-Duliere, M., (2000), Autocatalytic electroless nickel-boron plating on light alloys. *Surf. Coat. Technol.* 124, pp. 201-209
15. Henry, J.R., (2006), Electroless (autocatalytic) plating, *Met. Finish.* 104, pp.354-365
16. Riedel, W., (1991), Electroless nickel plating. finishing publications, Stevenage (UK).
17. Vitry V., Kanta A.-F., Dille J., and Delaunois F., (2012), Structural state of electroless nickel–boron deposits (5 wt.% B): characterization by XRD and TEM, *Surf. Coat. Technol.* 206, pp. 3444-3449
18. Delaunois, F., and Lienard, P., (2002), Heat treatments for electroless nickel-boron plating on aluminium alloys. *Surf. Coat. Technol.*, 160, pp. 139-148
19. Vitry V., and Delaunois F., (2015), Nanostructured electroless nickel-boron coatings for wear esistance, anti-abrasive nanocoatings, Elsevier, pp. 157-199
20. T. SAITO, O, E. SATO\*, M. MATSUOKA<sup>z</sup>, C. IWAKURA<sup>x</sup>, Electroless deposition of Ni-B, Co-B and Ni-Co-B alloys using dimethylamineborane as a reducing agent, *JOURNAL OF APPLIED ELECTROCHEMISTRY* 28 (1998) 559-563.
21. Satyajit Chatterjee <sup>a</sup>, S.M. Shariff <sup>c</sup>, G. Padmanabham <sup>c</sup>, J.Dutta Majumdar <sup>b</sup>, A. Roy Choudhary <sup>a,\*</sup>, Study on the effect of laser post-treatment on the properties of nanostructured Al<sub>2</sub>O<sub>3</sub>-TiB<sub>2</sub>-TiN based coatings developed SHS and laser surface alloying, *surface & coatings technology* 205 (2010) 131-138

22. D. Zois, A. Lekatou, M. Vardavoulias, A microstructure and mechanical property investigation on thermally sprayed nanostructured ceramic coatings before and after a sintering treatment, *surface & coatings technology* 204 (2009) 15-27.
23. Haihui Zhou, Qiang Yu, Qiling Peng, Hua Wang, Jinhua Chen, Yafei Kuang, Catalytic graphitization of carbon fibers with electrodeposited Ni-B alloy coating, *Materials Chemistry and Physics* 110 (2008) 434-439
24. Vaibhav Nemane, Satyajit Chatterjee<sup>1</sup>, Scratch and Sliding Wear Testing of Electroless Ni-B-W Coating, *Journal of Tribology*, FEBRUARY 2020, Vol. 142 / 021705-1
25. Vaibhav Nemane, Satyajit Chatterjee<sup>1</sup>; Nanomechanical, Tribological, and Scratch Properties of Electroless Ni-B-W Alloy and Ni-B-W-SiC Composite Coatings, *Journal of Tribology*, MAY 2022, Vol. 144 / 051402-1
26. Pal S., Verma N., Jayaram V., Biswas S.K. and Riddle Y., (2011), Characterization of phase transformation behavior and microstructural development of electroless Ni-B coating, *Mater. Sci. Eng. A* 528, pp 8269-8276
27. Madah F., Amadeh A. A., and Dehghanian C., (2016), Investigation on the Phase Transformation of Electroless Ni-B Coating After Dry Sliding Against Alumina Ball, *J. Alloys Compd.*, 658, pp. 272-279
28. Balaraju J.N., Narayanan T.S.N. S. and Seshadri S. K., (2003), Electroless Ni-P composite coatings *J. Appl. Electrochem.* 33, pp. 807-816
29. Yazdani, S., Tima, R. and Mahboubi, F., (2018), Investigation of wear behavior of as-plated and plasma-nitrided Ni-B-CNT electroless having different CNTs concentration, *Appl. Surf. Sci.* 457, pp. 942-955.
30. Lippert, T., Orтели, E., Panitz, J. C., Raimondi, F., Wambach, J., Wei, J., & Wokaun, A. (1999). ImagingXPS/Raman investigation on the carbonization of polyimide after irradiation at 308 nm. *Applied Physics A*, 69, S651-S654

31. Mather, R. R. (2009). Surface modification of textiles by plasma treatments. In Surface modification of textiles (pp. 296-317). Woodhead Publishing.
32. Guy, O. J., & Walker, K. A. D. (2016). Graphene functionalization for biosensor applications. *Silicon Carbide Biotechnology*, 85-141.
33. Jagannatham, M., Sankaran, S., & Prathap, H. (2015). Electroless nickel plating of arc discharge synthesized carbon nanotubes for metal matrix composites. *Applied Surface Science*, 324, 475-481.
34. Yim, Y. J., Rhee, K. Y., & Park, S. J. (2015). Influence of electroless nickel-plating on fracture toughness of pitch-based carbon fibre reinforced composites. *Composites Part B: Engineering*, 76, 286-291.